# Chapter 4

# Interacting Ions in Solution

Recently, the combination of near edge x-ray absorption spectroscopy (NEXAFS) with electronic structure calculations was used to study the hydrogen network in pure water [8, 62, 63] and in aqueous electrolytes [1, 64] as well as for the investigation of alcohol water mixtures [3, 65]. So far, all studies have focused on effects from the viewpoint of the solvent molecules by measuring oxygen 1s NEXAFS spectra. Understanding the nature of the hydrogen network in liquid water is of basic fundamental need in order to further investigate the behavior of the solute in the water, as well as other solvents. One of our recent study, which is not included in this thesis, depth selective photoelectron emission spectroscopy of liquid water as a function of energy [9] is done together with Hartee-Fock calculations. Briefly, this study shows that different $H_2O$ local environments can be identified by the oxygen 1s energy, which allows to quantitatively distinguish between strong and weak hydrogen bond configurations in the bulk, as well as free hydrogen oriented in the surface.

In the following sections the behavior of ions in solution will be discussed. In section 4.1 the evolution of the electronic structure locally at $Na^+$ ions in aqueous NaCl solution as a function of electrolyte concentration is investigated [66], in particular including high concentrations exceeding 1 M. NEXAFS has been used to experimentally study the local electronic structure at the $Na^+$ ion in the water. It turns out that there are clear spectral signatures related to the $Na - H_2O$ and Na-Cl interaction, which can be interpreted by theoretical modeling of the NEXAFS spectra. In section 4.2 the investigation is extended to study the effect of the solvent on the local geometrical and electronic structure of $Na^+$. NEXAFS spectra for 1 M NaI electrolyte in water vs. ethanol as the solvent are compared [67]. The comparison of experiment and theory allows to draw conclusions about the $Na^+$ $Cl^-$ interaction present in

the electrolytes. We will demonstrate that for the ethanol-based electrolyte, the observed NEXAFS structure is very well modeled by a $Na^+EtOH_6$ cluster. This situation is different in the water-based NaI electrolyte, where the comparison of experiment and theory suggests that both $Na^+(H_2O)_6$ and $Na^+(H_2O)_5I^-$ contribute significantly to the ensemble average, indicating the importance of $Na^+ - I^-$ interaction. In section 4.3, the effect of the pH on the local electronic structure of the $Na^+$ ion in water is investigated. A dramatic change in the $Na^+$ white line intensity in x-ray absorption is observed for high pH values, reflecting a changing local electronic structure at the $Na^+$ ions when $OH^-$ is present. Given the relative abundance of sodium and hydroxide ions, we will show that one $OH^-$ affects more than two $Na^+$ ions in an electronically noticeable way at pH 13. The experimental data are complemented by molecular dynamics simulations, which indicate the presence of structured clusters incorporating $Na^+$, $OH^-$, and solvent molecules. Furthermore, calculating the density-of-state using StoBe proves the assumption that the white line intensity would be affected by the existence of hydroxyl or hydronium ions in direct interaction with $Na^+$.

In section 4.4, the investigation has been extended from studying the alkaly metal ion in solution to transition metal ions in solution. A range from diluted (50 mM) to concentrated (1.5 M) aqueous $NiCl_2$ solutions is investigated in our study [68], where a transition in the importance of interionic interactions is expected. NEXAFS spectra for the $Ni^{2+}$ L-edge in aqueous $NiCl_2$ electrolyte solution will be presented as a function of the concentration, starting from the hydrated solid $NiCl_2.(H_2O)_6$. Two distinctive spectral features can be assigned as fingerprints of direct contact ion-pairs and solvent-shared ion-pairs in the solution. The spectra have been analyzed by the means of a charge transfer multiplet simulation [56,57, 69]. The multiplet approach has been extensively used in the analysis of L-edge spectra of transition metals, where it is established as a method for probing the metal ligand charge transfer [70–73]. As a complimentary investigation, the same range of concentration for $NiCl_2$ solution are investigated using resonant inelastic x-ray scattering (RIXS). Moreover, EXAFS is used to probe the changes in the first hydration shell around the $Ni^{2+}$ ions as a function of the concentration. The EXAFS spectra are modeled using the FEFF8 program package [74, 75].

# 4.1 Molecular and Electronic Structure in NaCl Electrolytes of Varying Concentration

*THE JOURNAL OF CHEMICAL PHYSICS 124, 114502 (2006)*

## 4.1.1 Introduction

Many theoretical and experimental methods have been used to investigate the behavior of ions in solution. Molecular dynamics (MD) simulations have been carried out in recent years in order to investigate the hydration structure and dynamical properties in aqueous solutions [76–79]. A recent MD study investigating the concentration dependent behavior of the solvated ions in aqueous NaCl solution indicates that $Na^+ - Cl^-$ pairs are relevant for electrolyte concentrations above 0.05 mol%, while conceding that it is difficult to pinpoint this concentration threshold exactly [80]. Molecular dynamics simulations predict the number of water molecules in the first hydration shell to be close to six and a Na-O distance around 2.3 Å. A concentration dependent theoretical study indicates a small but systematic decrease of water coordination with increasing NaCl electrolyte concentration without significant change in the Na-O radial distribution function [81].

The available experimental studies on the local coordination of water molecules around the $Na^+$ ion report coordination numbers ranging from four to eight [82–85], with newer studies predicting coordination between five and seven [86]. The salt concentration in these studies ranged from 1 M to 5.4 M, but the influence of concentration has neither been studied systematically nor does it show a clear trend across different investigations. Extended X-ray absorption find structure (EXAFS) spectra are capable of providing local structural information, providing a powerful tool in the analysis of the solvation structure of aqueous ionic solutions [87]. To our knowledge, no systematic EXAFS study or neutron diffraction study has been carried out as a function of concentration for ions in solution. For nearly saturated or supersaturated (6.18 M) aqueous solutions of NaCl a x-ray diffraction study reports a frequency factor of 0.3 for the occupation of a $Cl^-$ ion in direct contact (d(Na-Cl)=2.82 Å) with a $Na^+$ ion and an average hydration number of 4.6 for the $Na^+$ ion [88]. Recent experimental studies which probe the electronic structure not locally at the dissolved ions but either at the solvent molecules or throughout the $Na^+$ electrolyte found no evidence for ion-ion interaction for concentrations up to 4 M 1 [64, 89, 90]. On the other hand, measurements of the electrical

conductance in aqueous NaCl solution report a slightly less than tenfold increase in specific conductance when going from 0.01 M to 0.1 M NaCl [91], suggesting the existence of some ion association in this concentration range.

In this section, we address the evolution of the electronic structure locally at $Na^+$ ions in aqueous NaCl solution as a function of electrolyte concentration, in particular, including high concentrations exceeding 1 M. We use soft x-ray absorption spectroscopy to experimentally study the local electronic structure at the $Na^+$ ion in the solvent. It turns out that there are clear spectral signatures related to the $Na$–$H_2O$ and Na–Cl interactions. By comparing the experimental data to theoretical spectra based on the electronic structure calculations for a variety of model structures, we are able to exclude certain molecular arrangements put forward in the past. Furthermore, we discuss in a qualitative way the connection of a variety of structural models of the $Na^+$/solvent arrangement to the observed fingerprints based on the electronic structure calculations of the x-ray absorption spectra for these model structures.

### 4.1.2 Results and Discussion

In Fig.4.1, the change of the electronic structure at the $Na^+$ ion as a function of concentration is presented, as measured by NEXAFS of the $Na^+$ K-edge. The overall spectral shape is characterized by three peaks at 1072.8 eV, 1075 eV and 1080 eV, denoted A, B and C, respectively. In the lower concentration spectra one can discern two separate peaks B1 and B2 at around 1074.5 eV and 1076.3 eV within peak B. Changes in the spectral shape associated with the change in electrolyte concentration are observed. For increasing concentration, the intensity of peak B relative to peak C increases and B1 and B2 broaden, although an asymmetric peak shape is still visible up to a concentration of 4 M. With increasing concentration, peak A seems to increase in intensity. As the quantitative determination of the intensity of this comparatively weak spectral feature is strongly affected by the signal to noise ratio at low NaCl concentrations, we refrain from a quantitative evaluation of the evolution of peak A as a function of concentration. Another observable effect as a function of concentration is the shift of the energy position of peak C, which is shifted to lower absorption energies for increasing concentrations. The C-peak shift $E_C(M)$ and the B/C intensity ratio $I_{B/C}(M)$ scale approximately linear with the molarity M of the electrolyte as shown later in Fig.4.3.

As the effects in the experimental NEXAFS spectra are small, it is partic-

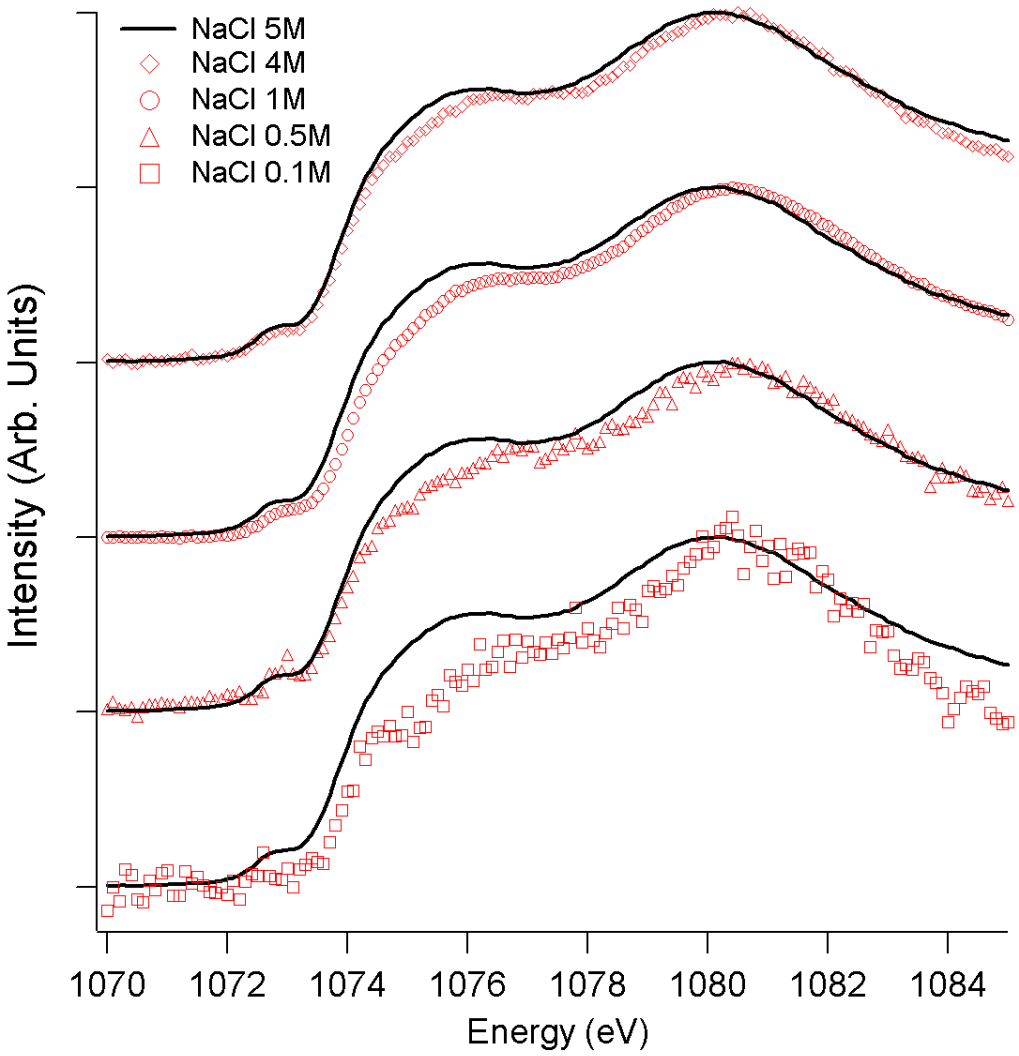


Figure 4.1: Sodium 1s NEXAFS spectra for different concentration of NaCl.aq solutions. The 5.0 M NEXAFS spectrum is superimposed on the other spectra as a solid line for easier comparison. Concentrations: 4 M (diamond, top), 1 M (sphere), 0.5 M (Delta), 0.1 M (box, bottom).

ularly important to exclude systematic errors in this measurement. For this reason the experiments have been carried out twice at different beam lines. The resulting spectra are identical within the statistical noise. Fluorescence yield measurements of the absorption coefficient can introduce artifacts which are connected to (spectroscopic) saturation effects in the detection technique; this is in particular the case for non-dilute, thick specimens [25]. The size of these distortions depends on the different contributions of the various atomic species to

the x-ray absorption cross-section as well as on the overall geometry. Following the treatment in Ref. [25], these saturation effects have been quantitatively simulated. Starting from the dilute 0.1 M case, we estimate that the saturation effect is not important, since the percentage concentration of $Na^+$ ions at this concentration is 0.2%. We thus identify the 0.1 M spectrum with $\mu(E)$, and simulate how this same $\mu(E)$ would look like with saturation at 5 M (if the electrolyte structure would not change). Input parameters for the simulation are the atomic absorption cross-sections as they are available on the Center of x-ray Optics web server. The result of this simulation is presented in Fig.4.2. The black line indicates a 0.75 eV Gaussian smoothed version of the 0.1 M data (black circles). The red line is the simulated distorted spectrum in fluorescence yield mode for 5 M concentration of NaCl, i.e. this is how the 0.1 M solution would look like at 5 M concentration if fluorescence yield saturation would be the only effect present. (Normal incidence of the x-rays, detection of fluorescence under a glancing angle of 30 degrees to the surface.). While some increase of intensity for low intensity regions of the NEXAFS spectrum is noticeable, it is also clear that this amount of spectral saturation cannot account for the experimentally observed differences between the 0.1 M and the 5 M NEXAFS spectrum. It is thus evident from the NEXAFS spectra in conjunction with this analysis that the electronic structure locally at the sodium atoms in the solution changes as a function of electrolyte concentration.

In Fig.4.3 the experimentally observed effects for the B/C intensity ratio and the energy shift of peak C as a function of concentration are compiled. Linear fits result in $E_C$= -0.115×M+7.96 and $I_{B/C}$=0.76×M+0.71, with M denoting the molarity of the solution ($I_{B/C} = 0.73 \times M + 0.71$ if the data is not corrected for spectral saturation). As will demonstrated below, both $\Delta E_C$ and $I_{B/C}$ are spectral fingerprints reflecting upon the sodium-water and sodium-chlorine distances in the electrolyte. To this end, an understanding of the origin of the spectral features in the NEXAFS spectra on the basis of electronic structure calculations for model clusters will be established.

An overview on the resulting calculated NEXAFS spectra for the model structures is presented in Fig.4.4. The dashed lines represent spectra calculated with the same inter-atomic distances within all different models, using minimum ionic radii as distances: d(Na-O)= 2.40 $\mathring{A}$ and - where applicable - d(Na-Cl)= 2.82 $\mathring{A}$. While this comparison highlights the spectral changes for a changing geometry, it is not a fair comparison to the experiment, as the inter-atomic distances have to be optimized within each model structure. The results of

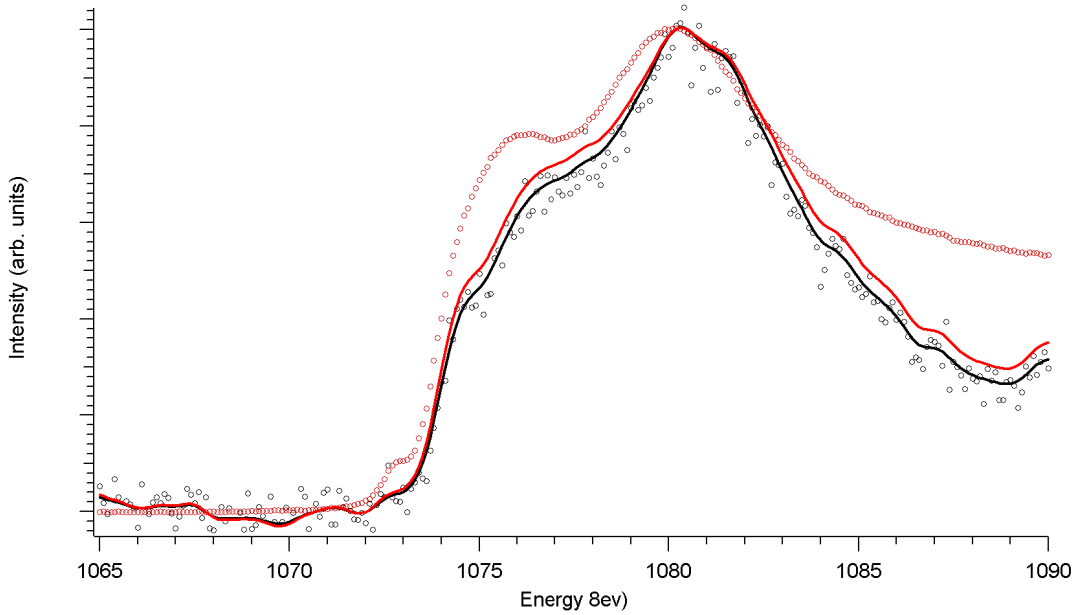


Figure 4.2: Simulation of the effects of spectral saturation due to the fluorescence yield detection mode. The black line (0.1 M spectrum with 0.75 eV Gaussian smoothing) is the input data obtained from the experimental data at 0.1M (black circles). If the electronic structure would not change as a function of concentration, the resulting FY-NEXAFS spectrum would look like the red line at 5M concentration, solely due to the influence of spectral saturation. This amount of distortion is insufficient to explain the shape of the NEXAFS spectrum observed in the experiment in a 5 M solution (red circles).

such an optimization with regard to the least square sum deviations between the theory and experiment are the spectra indicated by solid lines. Here, d(Na-O) has been systematically varied between 1.8 $\mathring{A}$ and 2.8 $\mathring{A}$ with 0.05 $\mathring{A}$ step size and d(Na-Cl) has been varied between 2.82 $\mathring{A}$ and 6.12 $\mathring{A}$ with 0.1 $\mathring{A}$ step size. In total, NEXAFS spectra for 740 model structures were calculated and evaluated. The resulting optimum parameters are listed in the caption of Fig.4.4. Even after the optimizing process, the overall spectral shape and the peak positions vary considerably between the models. The best agreement is found between the experimental data and the calculated spectrum based on the $Na^+(H_2O)_6$ and $Na^+(H_2O)_5Cl^-$ models. Note that the resulting sodium chlorine distances d(Na-Cl) in all models emerge to be 4 $\mathring{A}$ or larger, i.e. good agreement of a single model to the experimental data can only be obtained when $Cl^-$ influences the electronic structure on the

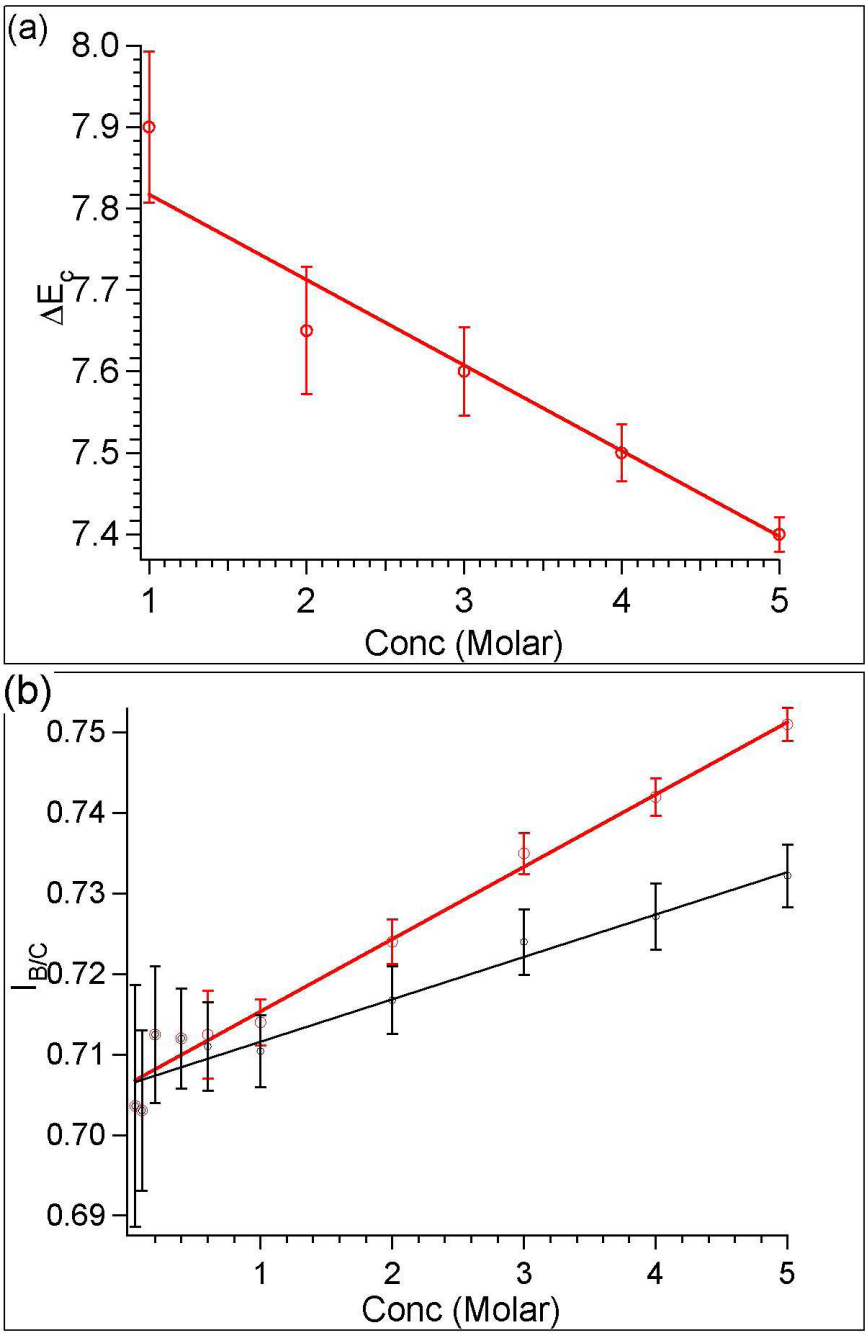


Figure 4.3: (a) Experimentally observed energy shift of peak C relative to peak A ($\Delta$EC) as a function of electrolyte concentration. (b) Experimentally observed intensity ratio of peak C to peak B ($I_{B/C}$) as a function of electrolyte concentration.

$Na^+$ site from a position beyond the first coordination shell. This is in line with the estimation of a frequency factor of only 0.3 for the occupation of a $Cl^-$ ion in direct contact (d(Na-Cl)=2.82 $\mathring{A}$) with a $Na^+$ ion in saturated aqueous NaCl solution by x-ray diffraction [82] and with recent findings on 4 M and 6.4 M aqueous solutions of $CaCl_2$, where a 'virtual absence' of $Ca^{2+}Cl^-$ contact ion pairs was reported, while an increase of solvent shared ion pairs was seen upon concentration increase at distances between 4.6 $\mathring{A}$ to 5.6 $\mathring{A}$ [92,93].

Both the relative intensities and the peak positions of the structures A, B and C are well reproduced in the $Na^+(H_2O)_6$ and $Na^+(H_2O)_5Cl^-$ models. In the $Na^+(H_2O)_6$ cluster, even the splitting of peak B as observed in the experimental data at lower concentration is visible. In contrast, the agreement of the spectra based on the $Na^+(H_2O)_4$, $Na^+(H_2O)_4Cl^-$ and $Na^+(H_2O)_5$ models with the experiment is particularly poor. This trend remains true upon small asymmetric variations of the $Na - OH_2$ bond distances, bond angles and $H_2O$ orientations. Based on this observation, those structures can only be minority contributions to the ensemble average; otherwise their contribution would be inconsistent with the experimentally observed NEXAFS spectrum. On the same basis, it is expected that the contributions of the $Na^+(H_2O)_6Cl^-$ and $Na^+(H_2O)_7$ structures to be relatively small. These expectations are in agreement with the average coordination of five to seven reported from structural probes and molecular dynamics [81, 82, 86]. In the following, $Na^+(H_2O)_6$ and $Na^+(H_2O)_5Cl^-$ are used as model clusters in order to qualitatively understand the dependence of the spectral fingerprints on the Na-O and Na-Cl distances.

In Fig.4.5, the evolution of the calculated NEXAFS spectra as a function of the relative atomic coordinates within the model structures $Na^+(H_2O)_6$ and $Na^+(H_2O)_5Cl^-$ are presented. In the $Na^+(H_2O)_6$ cluster, variation of the sodium water distance changes the intensity ratio of peak B to peak C, with larger $I_{B/C}$ for increasing $Na^+ - OH_2$ distance. A decreasing separation of the water molecules from the sodium ion leads to an increasingly pronounced splitting of peak B into B1 and B2. Experimentally, such behavior is observed for decreasing electrolyte concentration. In addition theory predicts an energetic shift of peak A. The spectral shape above 1080 eV x-ray energy is practically unaffected by the variation in inter-atomic distance. If $Na^+ - Cl^-$ interaction at distances corresponding to solvent-shared ion-pairs is included, as in the model $Na^+(H_2O)_5Cl^-$, the same general behavior will be observed: a change in the sodium water distance does only affect $I_{B/C}$ significantly. Again, $I_{B/C}$ decreases for decreasing interatomic separation, now, however, the

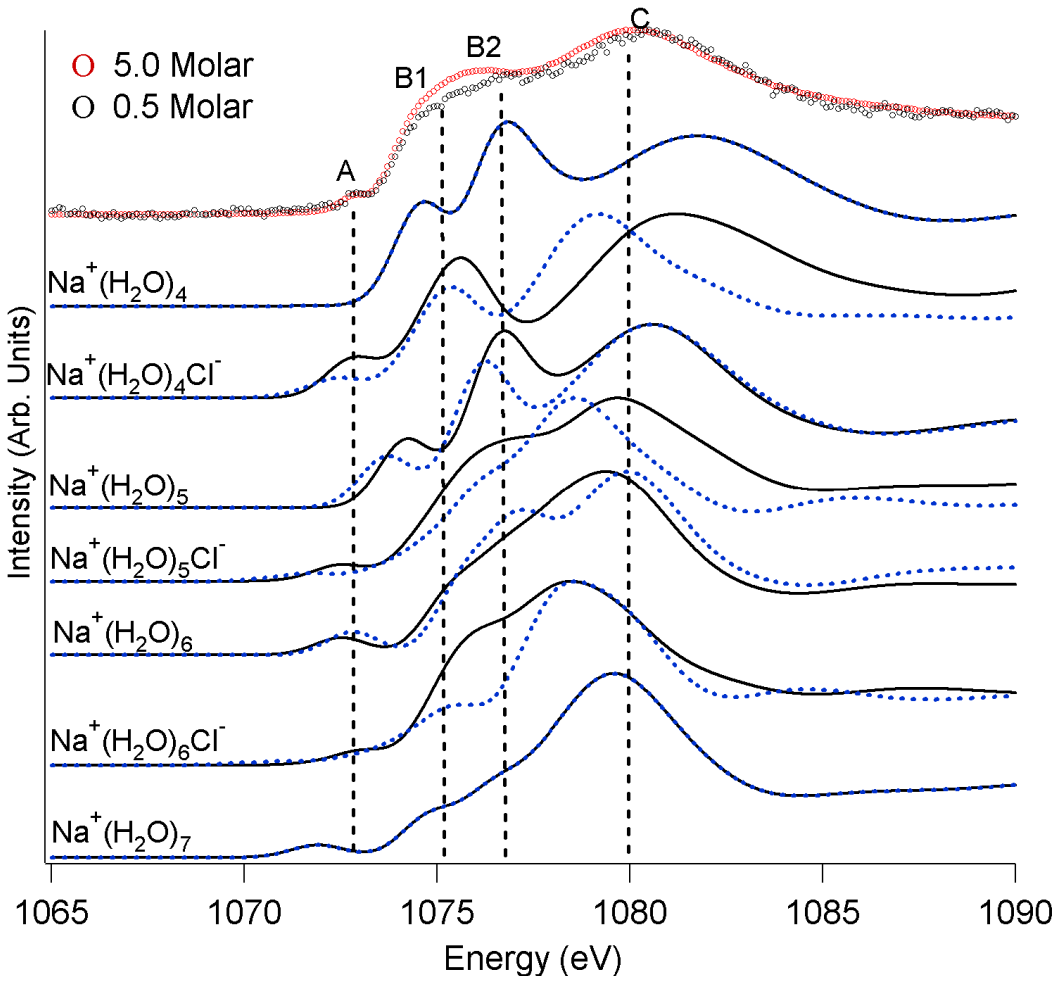


Figure 4.4: Calculated Na K-NEXAFS spectra for different model clusters. Spectra indicated by dashed blue lines are calculated spectra for minimum ionic radii with d(Na-O) = 2.4 $\AA$, d(Na-Cl) = 2.82 $\AA$. Spectra after bond length optimization based on a least square minimization with respect to the experimental data are shown as solid lines. The resulting distances for each cluster are as follows; $Na^+(H_2O)_4$ d(Na-O)= 2.4 $\AA$, $Na^+(H_2O)_4Cl^-$ d(Na-O)= 2.2 $\AA$, d(Na-Cl)= 5.1 $\AA$, $Na^+(H_2O)_5$ d(Na-O)= 2.5 $\AA$, $Na^+(H_2O)_5Cl^-$ d(Na-O)= 2.38 $\AA$, d(Na-Cl)= 3.9 $\AA$, $Na^+(H_2O)_6$ d(Na-O)= 2.5 $\AA$, $Na^+(H_2O)_6Cl^-$ d(Na-O)= 2.4 $\AA$, d(Na-Cl)= 4.0 $\AA$, $Na^+(H_2O)_7$ d(Na-O)= 2.4 $\AA$. Experimental spectra of 5.0 M (red) and 0.5 M (black) NaCl.aq have been included for direct comparison.

magnitude of the spectral change is different: for $Na^+(H_2O)_6$, we observe a $I_{B/C}$ increase of 0.210 $\pm$ 0.002 per 0.1 $\AA$ increase in $d(Na - OH_2)$, while a value of 0.200 per 0.1 $\AA$ is observed in the $Na^+(H_2O)_5Cl^-$ case. To this end,

one can conclude that upon variation of the sodium water distance, only $I_{B/C}$ changes, while in particular the energetic position of peak C ($\Delta E_C$) is unaffected.

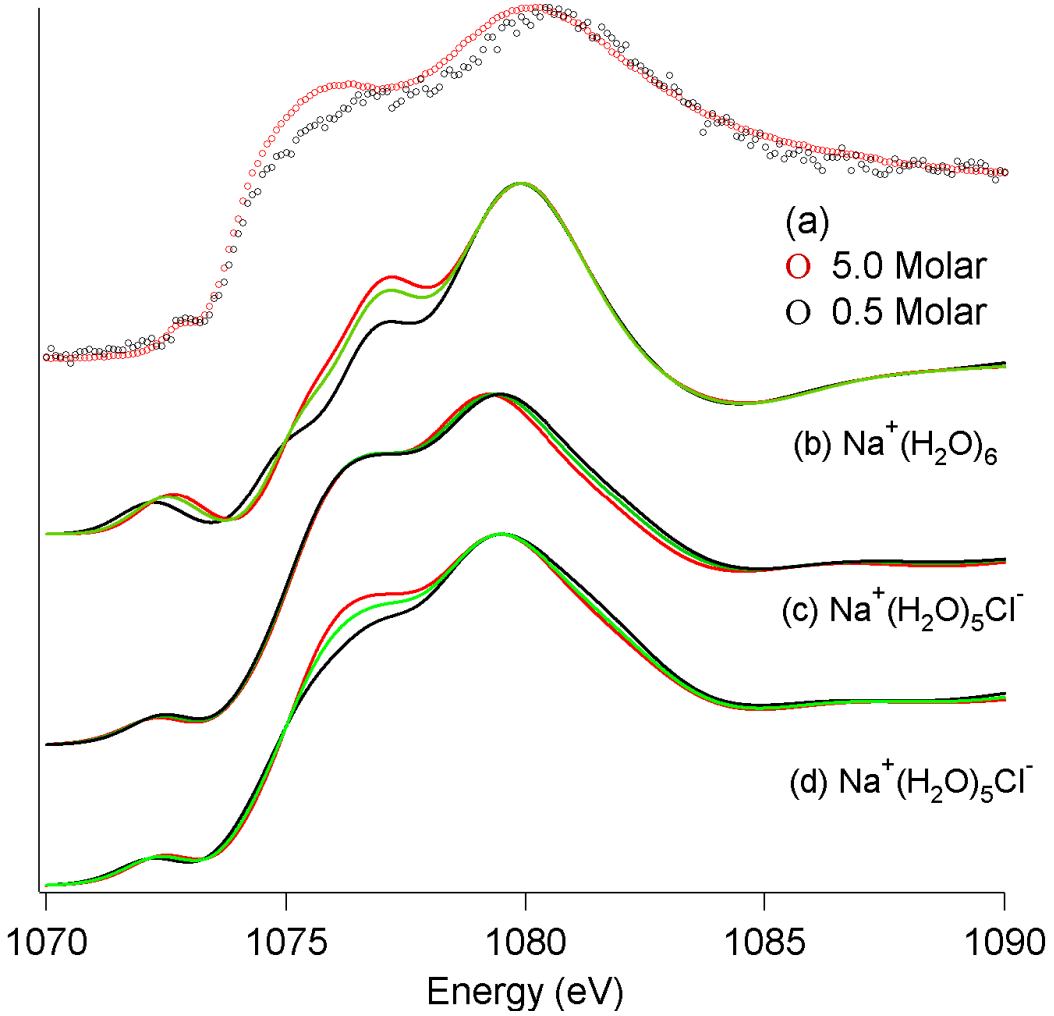


Figure 4.5: Changes in the calculated NEXAFS spectra upon systematic variation of atomic distances in selected model clusters. (b) $Na^+(H_2O)_6$ : d(Na-O)= 2.37 $\AA$ (black), 2.35 $\AA$ (green), 2.30 $\AA$ (red). (c) $Na^+(H_2O)_5Cl^-$ : Fixed d(Na-O)= 2.4 $\AA$ ; d(Na-Cl)= 3.5 $\AA$ (red), 3.6 $\AA$ (green), 3.7 $\AA$ (black). (d) $Na^+(H_2O)_5Cl^-$ : Fixed d(Na-Cl)= 3.7 $\AA$; d(Na-O)= 2.35 $\AA$ (black), 2.38 $\AA$ (green), 2.4 $\AA$ (red). Experimental spectra are included in (a) for direct comparison.

On the other hand, variation of the $Na^+ - Cl^-$ distance affects $\Delta E_C$. Furthermore, the calculations show that an energy shift of peak C is due to

variation of the inter-ionic distance, with a change of 0.095±0.003 eV in peak position per 0.1 $\mathring{A}$ change in inter-ionic separation in the $Na^+(H_2O)_5Cl^-$ cluster. The determined $I_{B/C}$ slopes as a function of separation are not significantly dependent of the broadening parameters of the model spectra but they do of course reflect the behavior in a specific model only. In the experimental situation, these slopes will result from an ensemble average over different structures. As $\Delta E_C$ is unaffected by the sodium water separation and $I_{B/C}$ unaffected by sodium chlorine distance, it is a particularly useful spectral fingerprint which in principle allows to separate effects due to d(Na-Cl) and $d(Na-OH_2)$. Before rationalizing the sensitivity of $I_{B/C}$ and $\Delta E_C$ to $d(Na-OH_2)$ and d(Na-Cl) by inspection of the molecular orbitals involved in the electronic transitions, the experimental results as a function of electrolyte concentration will be compared with the findings from the NEXAFS modeling.

The two parameters d(Na-Cl) and $d(Na-OH_2)$ in the model clusters $Na^+(H_2O)_6$ and $Na_+(H_2O)_5Cl^-$ are sufficient to describe the evolution of the spectral fingerprints $\Delta E_C$ and $I_{B/C}$ as a function of electrolyte concentration in our experimental spectra. The inter-ionic separation, on the other hand, is the only factor that produces an energy shift of peak C. The experimentally observed $\Delta E_C$ as a function of electrolyte concentration is consistent with a reduction of the d(Na-Cl) from 3.9 $\mathring{A}$ at a concentration of 1 M to 3.5 $\mathring{A}$ at 5 M, exhibiting a clear trend with concentration while still remaining in the solvent shared ion pair regime. While the magnitude of the d(Na-Cl) distance change dependent on the particular model cluster, one may expect the trend to an average reduced d(Na-Cl) for increasing concentration to be general, considering that a 6.14 M solution of NaCl in water is saturated at room temperature and ambient pressure and that solid NaCl with d(Na-Cl)=2.82 $\mathring{A}$ will precipitate for higher concentration. Pointing out that without interaction between the $Na^+$ and $Cl^-$, the experimentally observed trend in $\Delta E_C$ can not be explained in our models. This is a strong indication that ion-ion interaction in solvent shared ion pairs is important in NaCl electrolytes for concentrations of 1M and higher. This result is at variance with conclusions from a recent electron spectroscopy study of sodium iodide electrolytes, where no dependence of the electron binding energies in the occupied electronic states was found beyond a ±30 meV error level [90]. The fact that NEXAFS technique is looking at unoccupied states in the immediate vicinity of the HOMO-LUMO gap with high sensitivity to chemical binding and the bulk sensitivity of our experimental technique may explain this discrepancy. On the other hand, the conclusions in this study are in line with the aforementioned EXAFS and neutron diffraction results on the

$CaCl_2.aq$ system, which are to some extent comparable as the Pauling ionic radii of $Na^+$ and $Ca^{2+}$ differ by less than 4% [92, 93].

In order to clarify the mechanisms underlying the sensitivity of peak B and C toward water and chlorine interactions within the electrolyte solution, the Gaussian03 package [14] is used to analyze the molecular orbitals acting as final states in the Na 1s NEXAFS dipole transitions [18]. In the $Na^+(H_2O)_6$ cluster, the Na 1s orbital has $a_{1g}$ symmetry with respect to the entire $O_h$-symmetric cluster and the dipole operator is represented by $< t_u >$, allowing transitions to $t_u$ molecular orbitals. In the case of $Na^+(H_2O)_5Cl^-$, the Na 1s orbital has $a_1$ symmetry (in the $C_{2v}$-symmetric cluster) and the dipole operator is described by $< a_1 + b_1 + b_2 >$, resulting in possible dipole transitions to unoccupied molecular orbitals characterized by $a_1$, $b_1$ and $b_2$ symmetry. The small spectral weight of peak A precludes us from utilizing this peak as a reliable spectral fingerprint, especially given the limited signal to noise ratio for low concentration electrolytes. This situation is different for peaks B and C, where the final state molecular orbitals posses significant electron probability of suitable symmetry locally at the sodium site, resulting in a higher transition probability.

Two types of molecular orbitals dominate peak B in the $Na^+(H_2O)_6$ structure, as shown in Fig.4.6. Little overlap between the unoccupied $a_1 - type$ orbitals localized on the oxygen atoms and the unoccupied states centered at the sodium site is found in the molecular orbital shown in (a), giving rise to feature B1 in the spectra. In comparison, significantly larger overlap in the state is giving rise to B2, shown in (b). As a result, peak B splits in the experimental spectra and is sensitive in its intensity to the sodium oxygen distance. The interaction between sodium and chlorine ions giving rise to the energetic shift of peak C is mediated by the molecular orbital for the $Na^+(H_2O)_5Cl^-$ cluster shown in (c), where the lobe of p-type orbital on the sodium ion is strongly extended toward the chlorine ion.

### 4.1.3 Conclusion

From this investigation, the combination of NEXAFS spectroscopy with electronic structure calculations allows us to understand the origin of spectral fingerprints which are sensitive to the sodium-water and sodium-chlorine distance in NaCl electrolytes. The inclusion of inter-ionic interaction as in the $Na^+(H_2O)_5Cl^-$ cluster, where $Na^+$ and $Cl^-$ form a solvent shared ion pair, is

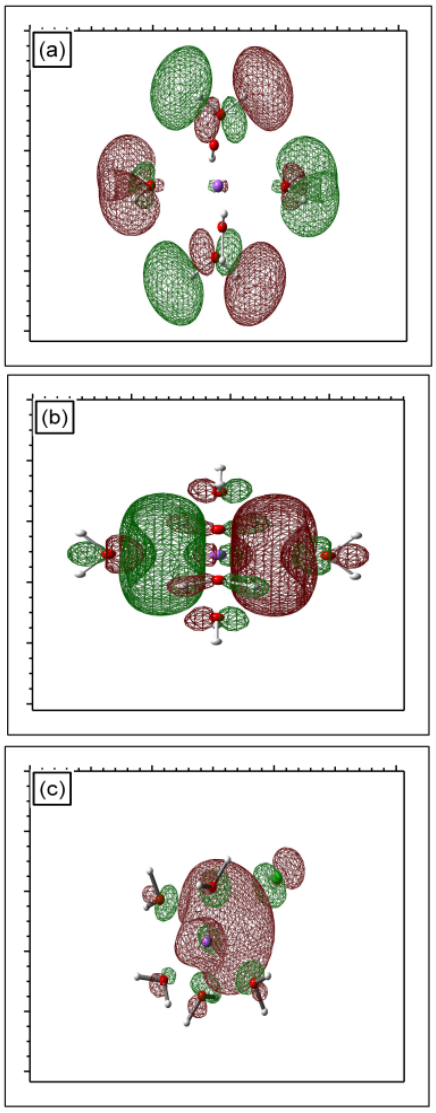


Figure 4.6: Visualization of unoccupied orbitals involved in the NEXAFS transitions at different transition energies. (a) LUMO+6 orbital contributing to the B1 peak in the $Na^+(H_2O)_6$ cluster, (b) LUMO+17 orbital contributing to the B2 peak in the $Na^+(H_2O)_6$ cluster, (c) LUMO+14 orbital contributing to peak C in the $Na^+(H_2O)_5Cl^-$ cluster.

important for a quantitative understanding of the NEXAFS spectra, in particular for concentrations above 1 M. Upon increasing the concentration from 1 M to 5 M solution, the comparison of experiment and theory for the $Na^+(H_2O)_5Cl^-$ cluster suggests a decrease of the average $Na^+ - Cl^-$ distance, which in this model cluster amounts to about 10%.

## 4.2 Steric Hindrance of Ion-Ion Interaction in Electrolytes

*PHYSICAL REVIEW B 73, 075120 (2006)*

### 4.2.1 Introduction

Further detailed information on the interionic interaction as well as on the influence of solvents on this interaction is desirable. In this section, we compare Na 1 s NEXAFS spectra of 1 M NaI electrolyte with water vs ethanol as the solvent. The experimental results are compared to simulated spectra based on electronic structure calculations, carried out by density functional theory for different model clusters. The comparison of experiment and theory allows us to draw conclusions about the $Na^+$ $Cl^-$ interaction present in the electrolytes.

### 4.2.2 Results and Discussions

In Fig.4.7, the experimental Na 1s NEXAFS spectra for one molar solutions of NaI in water and in ethanol are showen. A clear difference in the NEXAFS spectra is observed, reflecting a different electronic structure locally at the Na ions depending on the solvent. In the immediate near edge region, three peaks can be discerned for the case of ethanol as a solvent, which are labeled A through C. In the case of water as a solvent, these structures are shifted to higher absorption energies as compared to the situation in ethanol. Furthermore, a shoulder develops at peak B, and the resulting features are labeled as B1 and B2.

The electronic structure and the resulting NEXAFS spectra are calculated by DFT using the StoBe deMon code are compared to the experimental ones. In a previous chapter where the concentration dependent study for aqueous NaCl electrolytes is demonstrated, $Na^+(H_2O)_6$ clusters in $O_h$ symmetry and $Na^+(H_2O)_5Cl^-$ clusters in $C_{2v}$ symmetry are shown to result in the best agreement of experimental NEXAFS spectra and StoBe model calculations. In particular, the experimental NEXAFS spectra for high electrolyte concentrations require $Na^+Cl^-$ interaction as in the $Na^+(H_2O)_5Cl^-$ cluster in order to describe the experimental observations well [66].

Based on these earlier results, the $Na^+$ environment in solution is modeled with the following high symmetry structures of the first hydration shell (i) $Na^+(H_2O)_5$ in trigonal bipyramidal symmetry, (ii) $Na^+(H_2O)_6$ in $O_h$ symmetry,

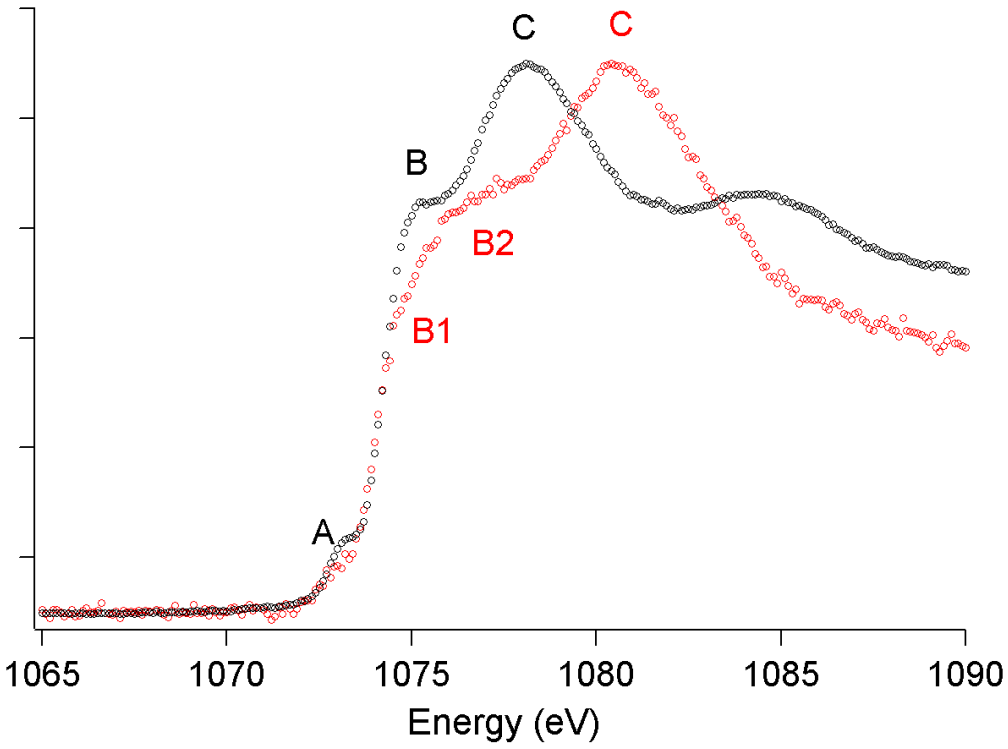


Figure 4.7: Na K-NEXAFS spectra for 1 molar solutions of NaI in water (red circles) and ethanol (black squares).

and (iii) $Na^+(H_2O)_5I^-$ in $C_{2v}$ symmetry. In the case of NaI in ethanol NEXAFS spectra are calculated for a $Na^+(EtOH)_6$ cluster (with the oxygen atoms in ethanol in $O_h$ symmetry with respect to the $Na^+$ ion), for $Na^+(EtOH)_5I^-$ (with the $I^-$ ion and the oxygen atoms in ethanol in $C_{2v}$ symmetry with respect to $Na^+$), and for a $Na^+(EtOH)_5$ cluster (with the oxygen atom in the ethanol molecules in trigonal bipyramidal symmetry around the $Na^+$ ion). In these calculations, the sodium oxygen distance d(Na-$OH_2$) was varied between 2.3 $\mathring{A}$ and 2.6 $\mathring{A}$, which is the range indicated by x-ray diffraction [82, 88], and, where applicable, the sodium iodine distance d(Na-I) was varied between 3.5 $\mathring{A}$ and 6.5 $\mathring{A}$. To further study interionic interactions, a $Na^+(EtOH)_6$ cluster with and without an additional $I^-$ in the second hydration shell are calculated at 6.4 $\mathring{A}$ distance from the $Na^+$ ion. Of course, the situation encountered in the real electrolyte is a complex and dynamic mix of many local structures. In other words, the electrolyte is not made up exclusively by $Na^+(H_2O)_6$ or $Na^+(H_2O)_5Cl^-$ clusters, but one can extract useful information on the experimental data by comparison with these models by investigating trends

resulting under systematic variation of the model geometry.

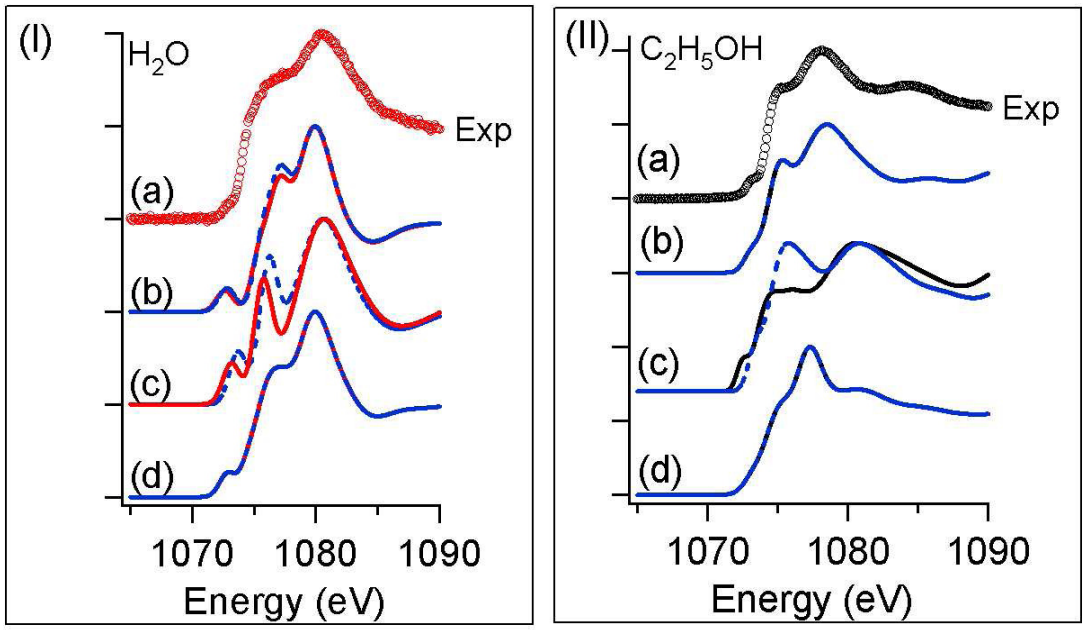


Figure 4.8: Calculated Na K-NEXAFS spectra for different model clusters compared to the experimental data, shown in (a). (I) The case of $H_2O$ as a solvent, the dashed blue line indicates results for a fixed set of bond lengths: d(Na-O)=2.4 $\AA$ and d(Na- I) = 4.8 $\AA$, where applicable. The red solid line indicates spectra after optimization of the bond lengths for each model as follows: (b) $Na^+(H_2O)_6$ $O_h$ symmetry with d(Na-O)=2.42 $\AA$ (LSS=0.021), (c) $Na^+(H_2O)_5$ $T_h$ symmetry with d(Na-O)=2.25 $\AA$ (LSS=0.031), (d) $Na^+(H_2O)_5I^-$ $C_{2V}$ symmetry with d(Na-O)=2.4 $\AA$ and d(Na-I)=4.8 $\AA$ (LSS=0.012). (II) The case of ethanol as a solvent, the dashed blue line indicates results for a fixed set of bond lengths, d(Na-O)=2.47 $\AA$ and d(Na-I)=4.8 $\AA$, where applicable. The black solid line indicates spectra after optimization of the bond lengths for each model as follows: (b) $Na^+(EtOH)_6$ with oxygen atoms in $O_h$ symmetry around the $Na^+$ with d(Na-O)=2.47 $\AA$ (LSS=0.003), (c) $Na^+(EtOH)_5$ where oxygen in $T_h$ symmetry around $Na^+$ with d(Na-O)=2.3 $\AA$ (LSS=0.013), (d) $Na^+(EtOH)_5I^-$ where the oxygen atoms are in a $C_{2V}$ symmetry around $Na^+$ with d(Na-O)=2.5 $\AA$ and d(Na-I)=4.8 $\AA$ (LSS=0.020).

The calculated spectra for each cluster are presented in Fig.4.8. To compare the influence of the cluster symmetry, first NEXAFS spectra are calculated for identical bond length for all symmetries, namely with d(Na-O) = 2.40 $\AA$ for

water and d(Na-O) = 2.47 $\mathring{A}$ for ethanol as a solvent. The resulting spectra are indicated by dashed lines. For both solvents, the agreement between theory and experiment seems better for the models with sixfold coordinated sodium ions than for lower or higher coordination. To allow a more quantitative comparison between experiment and theory, the bond lengths within each model were determined by systematic variation and least square fitting of the calculated spectra to the experimental data. The optimum bond lengths and associated least square sums (LSS) are listed in the figure caption; the resulting spectra are shown as solid lines in Fig.4.8. In the case of water as a solvent, the best agreement is found between the experimental data and the calculated spectrum based on the $Na^+(H_2O)_5I^-$ model (LSS=0.012). Both the relative intensities and the peak positions of the structures A, B and C are well reproduced. The LSS for the $Na^+(H_2O)_6$ cluster calculation (LSS=0.021) is somewhat larger than the respective value for $Na^+(H_2O)_5I^-$, but this model does reproduce the weak splitting of peak B as observed in the experimental data. The resulting $Na^+$-O optimum bond length d(Na-O) is 2.42 $\mathring{A}$ in the $Na^+(H_2O)_6$ model and 2.4 $\mathring{A}$ in the $Na^+(H_2O)_5I^-$ model. This range is in agreement with cation-oxygen radial distribution function obtained by calculating the potential energy surface with respect to d($Na^+$-O) for the $O_h$ cluster by a molecular dynamics approach [94]. For the $Na^+(H_2O)_5I^-$ cluster, the best agreement with the experimental data is obtained for d(Na-I)= 4.8 $\mathring{A}$, with the first hydration shell of water around the $Na^+$ ion located at a distance between 2.3 $\mathring{A}$ and 2.4 $\mathring{A}$. The iodine ion is thus located in a distance corresponding to the second $H_2O$ hydration shell and together with the $Na^+$ ion can be regarded as a solvent shared ion pair, similar to the situation found in the aqueous $Ca^{2+}/Cl^-$ electrolytes [92, 93].

The comparison between experiment and theory for the case of ethanol as a solvent is presented in the second panel of Fig.4.8. In contrast to the case of water as a solvent, the agreement of the model with pure, six fold solvent molecule coordination to the experimental data (LSS=0.003) is significantly better than the $Na^+(EtOH)_5I^-$ model (LSS=0.020). In particular, the B/C peak intensity ratio in the $Na^+(EtOH)_5$ model calculation disagrees with the experimentally observed one and this particular configuration cannot contribute more than 5% to the ensemble average. Calculations of NEXAFS spectra for clusters with less than five or more than six ethanol molecules around a $Na^+$ ion results in even stronger disagreement with the experimental data (not shown). In all models, of the oxygen atom within the ethanol molecule is oriented toward the $Na^+$ ion while the hydrocarbon chain is pointing away from the $Na^+$ ion; other orientations show poorer agreement to the experimental NEXAFS spectra.

As mentioned above, the best agreement between the experimental and calculated spectra is obtained in the $Na^+(EtOH)_6$ cluster model. In the $Na^+(EtOH)_5I^-$ model, we have checked radial distances $d(Na^+ - O)$ from 2.3 A to 2.5 $\mathring{A}$ with d$(Na^+ - I^-)$ covering the interval from 3.5 $\mathring{A}$ to 5.5 $\mathring{A}$. The best agreement to the experimental data is obtained for the spectrum shown in Fig.4.8(d), with a LSS that is three times larger than the spectrum based on the pure solvent model in (a). This finding demonstrates that $Na^+ - I^-$ interaction is much less important in the 1 M ethanol-based electrolyte as compared to the aqueous solution. The sodium oxygen distance d(Na-O)= 2.47 $\mathring{A}$ in the $Na^+(EtOH)_6$ model is larger than in the equivalent water structure, which seems reasonable due to the lower amount of partial charge on the oxygen atom in the ethanol molecule as compared to water. In addition, steric interaction of the larger ethanol molecules may lead to an increase of d(Na-O) in the first hydration shell as compared to the case of water as a solvent.

For the model structures tested, better agreement between experiment and theory is obtained for the case of ethanol as a solvent as compared to water as a solvent. Given the smaller size of the water molecule compared to ethanol, the inclusion of a second coordination shell in the models is more important in the water case. While the discrepancy between experiment and theory can be reduced in particular for the water case by modeling more than one hydration shell, the associated calculation of the electronic structure and the NEXAFS spectrum becomes very complex and is outside the scope of this study.

For larger interionic distances in the $Na^+(EtOH)_5I^-$ model, the influence of interionic interaction by placing the $I^-$ outside a $Na^+(EtOH)_6$ cluster is tested, i.e. where the sodium ion is surrounded by a 'complete' EtOH coordination shell. As shown in Fig.4.9, very small changes in the calculated spectral shape (LSS=0.0030 vs. 0.0028) at such interionic distances. In combination with the results presented in the context of Fig.4.8, ethanol efficiently excludes $I^-$ ions from the first hydration shell at 1 M concentration. Note that in the water case, the best agreement within the $Na^+(H_2O)_5I^-$ model for d(Na-I)= 4.8 $\mathring{A}$. At this distance, one can expect the steric hindrance by water molecules to be small compared to the situation encountered in ethanol.

Keeping in mind that the experiment is probing a spatial and temporal ensemble average, this different behavior in the two solvents should be reflected in the respective residence times of solvent molecules. We are not aware of

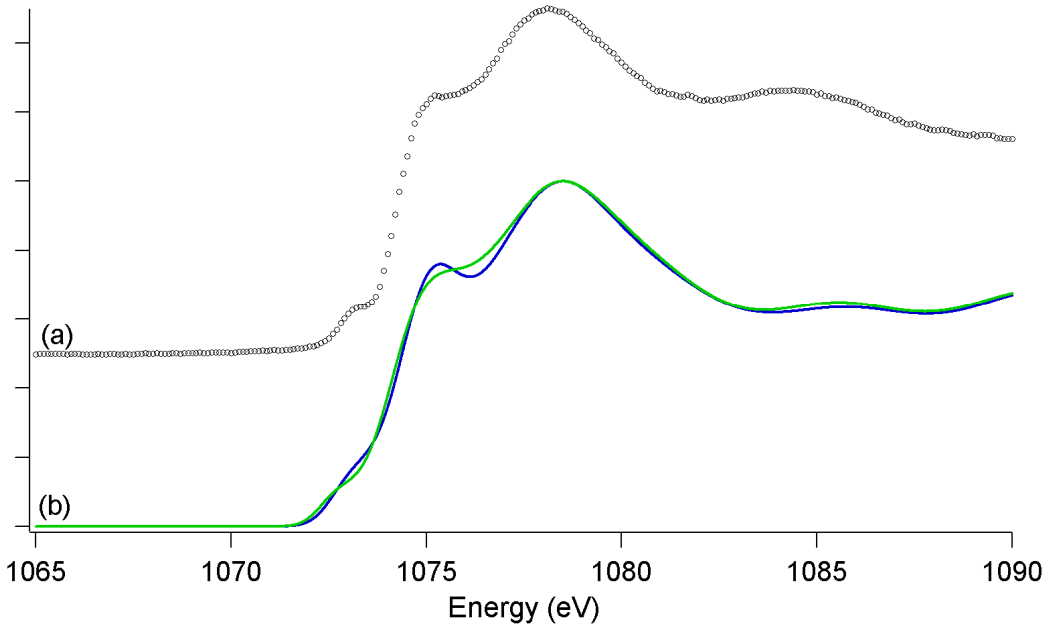


Figure 4.9: Effect of presence of the $I^-$ anion outside of the first hydration shell on the calculated Na K-NEXAFS spectra: (a) Experimental NEXAFS for 1 M NaI in ethanol and (b) Calculated spectra for a $Na^+(EtOH)_6$ cluster (solid blue line) and a $Na^+(EtOH)_6I^-$ cluster (dashed black line) with d(Na-I)=6.4 $\mathring{A}$ and d(Na-O)=2.47 $\mathring{A}$ in both cases.

a molecular dynamics calculation comparing water and ethanol. For water vs. methanol a molecular dynamics (MD) calculation predicts about half the residence time for methanol as compared to water [94]. If similar residence time for methanol and ethanol is assumed (which both carry one OH functional group), the experimental results regarding d(Na-O) exhibit a trend which is in agreement with the theoretical predictions for the HOH/MeOH case.

The existence of a double structure in peak B is in the case of water as a solvent, which is absent in the respective sodium spectra when ethanol is the solvent. To this end, the electronic structure in the $Na^+(H_2O)_6$ model is analyzed, where the spectrum does exhibit the double peak structure in contrast to the $Na^+(EtOH)_6$ situation. Inspecting the electronic wave functions, two different types of orbitals give rise to the double structure in the water case. Two representative wavefunctions are visualized in the first panel of Fig.4.10. With respect to the oxygen atom in the water molecule they exhibit $a_1$ vs. $b_2$ symmetry. In contrast, only one type of orbital (a‘ symmetry) contributes to peak B in

the case of ethanol as a solvent. For completeness, the respective orbitals for the $Na^+(H_2O)_5I^-$ model are shown as well. The presence of the $I^-$ ion does not change the general picture: again, two types of orbitals $(b_1, b_2)$ are present, the energy separation, however, is reduced compared to the $Na^+(H_2O)_6$ case and a splitting is therefore not noticeable given the amount of broadening in the spectra.

The molecular orbitals contributing to peak C are presented in Fig.4.11. For the $Na^+(H_2O)_5I^-$ cluster model, the p-orbital on the $Na^+$ is hybridized and forming a sp-orbital, which is strongly overlaping with the p-orbital of $I^-$. This makes peak C sensitive to the ion interaction as presented in Fig.4.1. By replacing the anion of this cluster model by a water molecule, the p-orbital gets localized (and not hybridized) on the $Na^+$ site, as shown in Fig.4.11III. Moreover, replacing the water molecules by ethanol in the first hydration shell of $Na^+$, an overlap between the p-orbital of the sodium with A' molecular orbital of the ethanol is created. This strong overlap hinders the electronic interaction between the $Na^+$ and the possible counter anions which may exist outside the first hydration shell.

### 4.2.3 Conclusion

In conclusion, Na 1s NEXAFS spectra of 1 M solution of NaI in water and ethanol are presented. Clear solvent-dependent differences in the local electronic structure are observed. The experimental data are compared to calculated spectra based on DFT calculations, including the effect of the core hole on the NEXAFS spectra. For the ethanol based electrolyte, the observed NEXAFS structure is very well modeled by a $Na^+(EtOH)_6$ cluster. Inclusion of an iodine ion in the first hydration shell leads to significant disagreement of the calculated and experimental spectra. An anion residing in the first hydration shell of the sodium ion contributes only negligibly to the ensemble of structures encountered in the ethanol based electrolyte. This 'exclusion' from the first hydration shell is due to steric hindrance by the solvent molecules. This situation is different in the water-based NaI electrolyte, where the comparison of experiment and theory suggests that both $Na^+(H_2O)_6$ and $Na^+(H_2O)_5I^-$ contribute significantly to the ensemble average, indicating the importance of $Na^+ - I^-$ interaction in particular at elevated concentrations of 1 M and above.

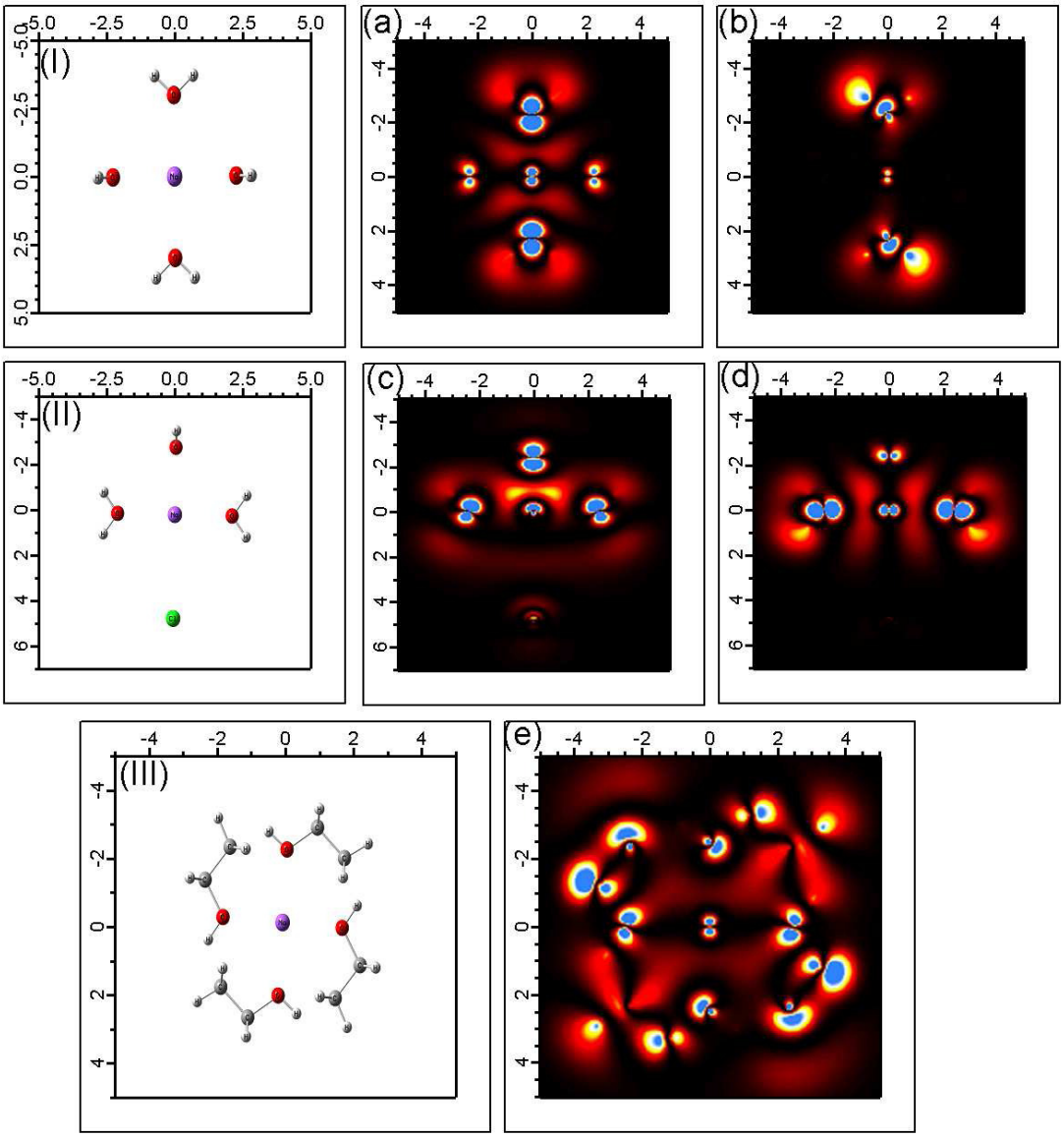


Figure 4.10: Orbitals contributing to the unoccupied states giving rise to peak B. Shown in (a) and (b) are representative orbitals of the $Na^+(H_2O)_6$ cluster contributing to peaks B1 and B2, respectively. Shown in (c) and (d) are representative orbitals of the $Na^+(H_2O)_5I^-$ cluster contributing to peaks B1 and B2, respectively. (e) Representative orbital of the $Na^+(EtOH)_6$ cluster contributing to peak B. Models are shown in a plane (molecules above and below are not shown); electron density is shown for the same plane. Lateral distances are in units of $\mathring{A}$.

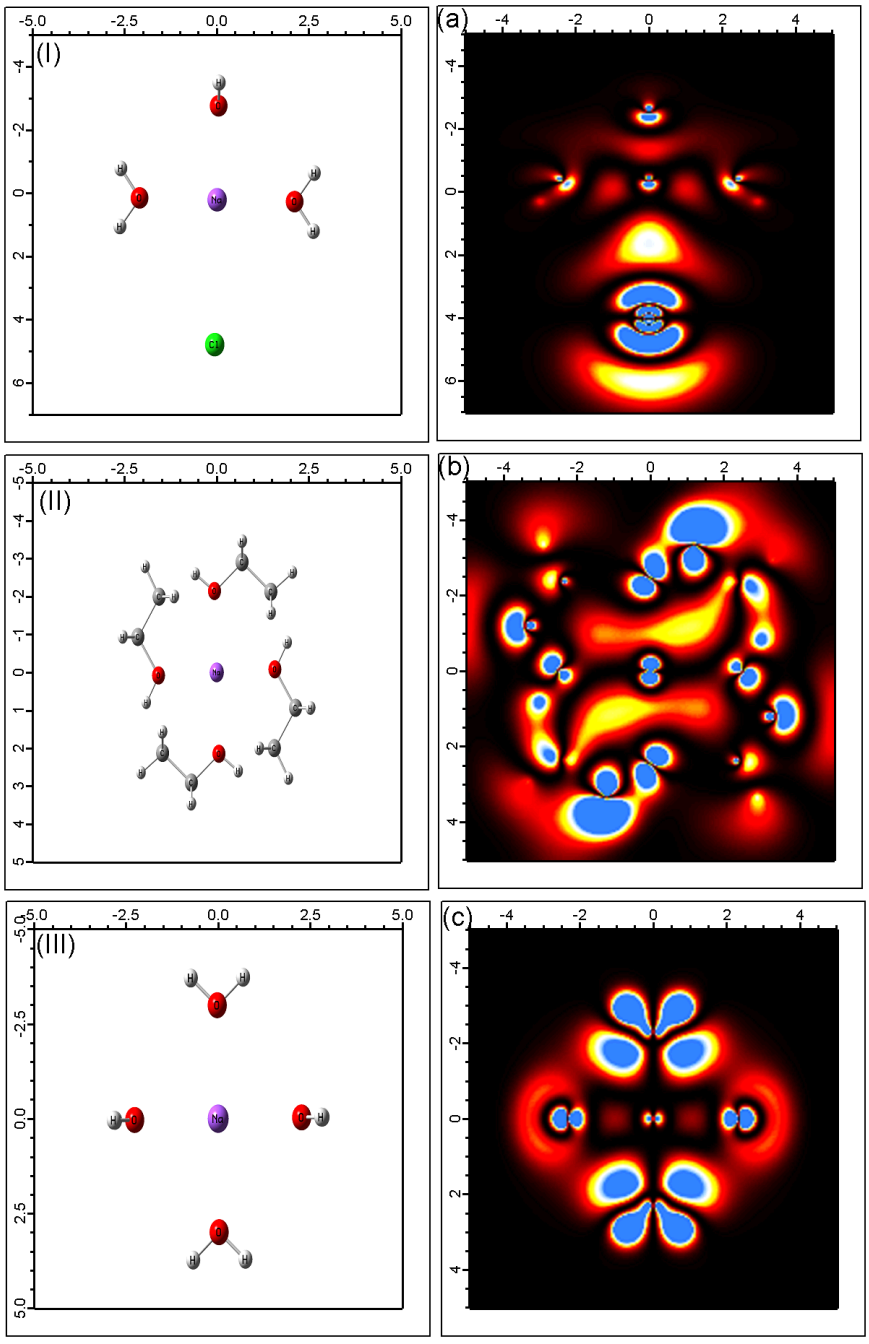


Figure 4.11: Orbitals contributing to the unoccupied states giving rise to peak C. Shown in (a) and (c) are representative orbitals of the $Na^+(H_2O)_5Cl$ and $Na^+(H_2O)_6$ cluster respectively. Shown in (b) is the corresponding one of $Na^+(EtOH)_6$. Models are shown in a plane (molecules above and below are not shown); electron density is shown for the same plane. Lateral distances are in units of $\mathring{A}$.

## 4.3 Density of States of $Na^+$ Ions as a Function of the Solution pH

*JOURNAL OF PHYSICAL CHEMISTRY B (2007) in press*

### 4.3.1 Introduction

Here, we focus on the electronic structure of solvated sodium ions, investigating the structure of aqueous NaCl as a function of pH. Long-range structuring in neat water, albeit invoked numerous times in the literature, most likely does not occur due to the remarkable ability of water molecules to reorient fast in the liquid. In concentrated salt solutions (e.g., NaCl) intermediate size structures can build up as a result of ion-pairing and clustering. An even more interesting situation occurs upon adding a strong base, such as NaOH, since hydroxide ions are not spherically symmetric and could form extended anisotropic networks of ions. This situation, which is explored in the present study, can have important consequences for physical and chemical processes in electrolytes, ranging from binding of ions to proteins to reactions in aqueous aerosols.

### 4.3.2 Results and Discussion

The local electronic structure at solvated $Na^+$ ions in 1 M aqueous NaCl solutions is investigated as a function of pH. In Fig.4.12, NEXAFS spectra are presented for 1 M aqueous solutions of NaCl at pH 1.9, pH 7.0, pH 8.5, pH 9.9, pH 11.5, pH 12.2, and pH 13.0. The pH was varied by adding concentrated HCl or NaOH solution, resulting in the ion concentrations listed in Table. 4.1. The solutions were prepared using water deionized immediately prior to the NEXAFS measurements. The pH was checked with a pH-meter before and after the measurements.

The absorption intensity shown in Fig.4.12 has been normalized to the incident photon flux, keeping the overall experimental condition exactly the same. As a result, the overall changes in intensity are meaningful. To exclude systematic errors, the data has been acquired several times with ascending and descending concentration series, yielding identical results; two datasets for each pH are shown in Fig.4.12.

The general spectral shape is characterized by four peaks at 1072.8, 1075, 1080, and 1110 eV, denoted A, B, C, and D respectively. This structure is

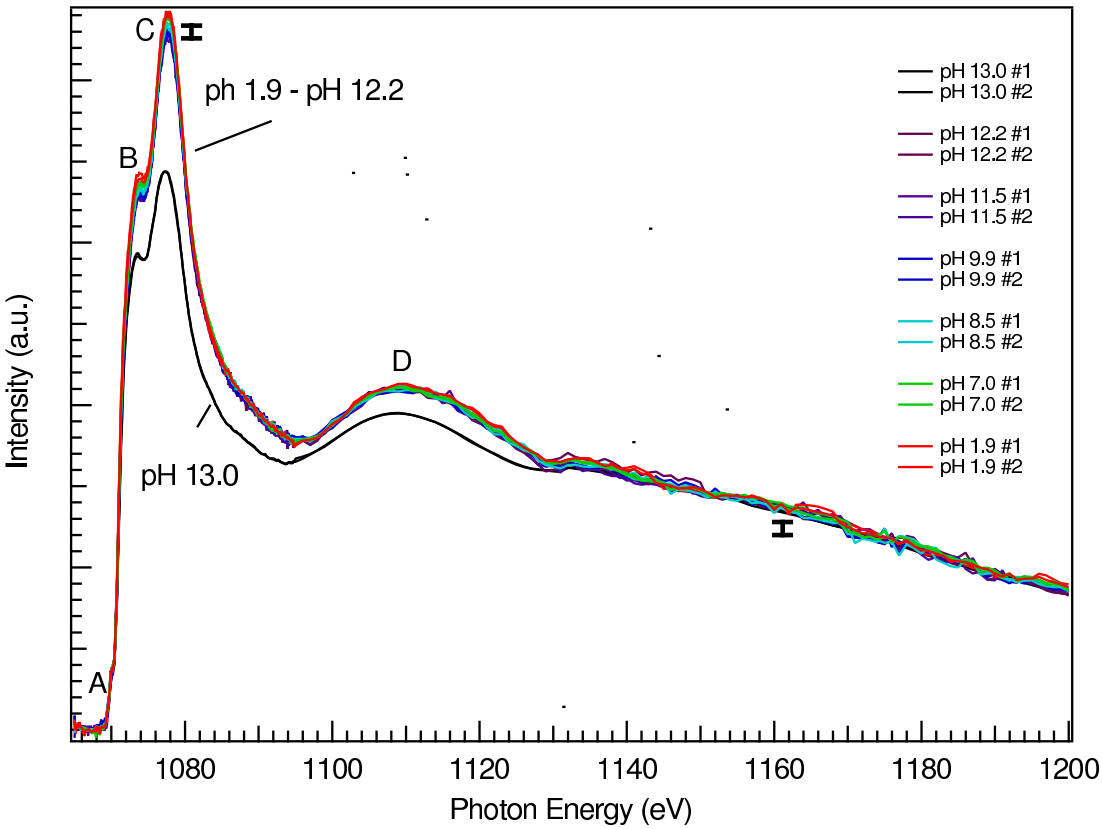


Figure 4.12: Na K-edge FY-XANES spectra for approx. 1 M NaCl solutions recorded at different pH values. Exact concentrations are listed in Table 4.1.

typical for the Na K-NEXAFS spectra of NaCl solutions [66, 67]. With the exception of the spectrum at pH 13.0, only minor changes in the absorption intensity as defined by the intensity integral under the peaks A-C are observed. In Table 4.1, the ion concentrations in the solution are listed. While at pH 7 only $Na^+$ and $Cl^-$ ions are present in appreciable concentration in the water, the concentration of $H^+$ and $OH^-$ increases when going to acidic/basic conditions.

As the Na 1s x-ray absorption edge is well described in a single electron picture and in dipole approximation, the spectra in the region of the peaks A-C reflect the unoccupied density of p-type states locally at the sodium atoms (p-DOS). [18] As a result, the white line intensity above the non-resonant background is proportional to the total number of empty states of p symmetry in the integration interval. This fact gives rise to the intensity sum rule for the number of valence holes in x-ray absorption. [18]. Even if electron correlation was present, the redistribution of spectral intensity occurs typically within

| | $[Na^+]$-1 | $[Cl^-]$-1 | $[H^+]$ | $[OH^-]$ |
|---|---|---|---|---|
| pH 1.9 | 0 | $1.26\times10^{-2}$ | $1.26\times10^{-2}$ | $7.94\times10^{-13}$ |
| pH 7.0 | 0 | 0 | $1\times10^{-7}$ | $1.0\times10^{-7}$ |
| pH 8.5 | $3.16\times10^{-6}$ | 0 | $3.16\times10^{-9}$ | $3.16\times10^{-6}$ |
| pH 9.9 | $7.94\times10^{-5}$ | 0 | $1.26\times10^{-10}$ | $7.94\times10^{-5}$ |
| pH 11.5 | $3.16\times10^{-3}$ | 0 | $3.16\times10^{-12}$ | $3.16\times10^{-3}$ |
| pH 12.2 | $1.58\times10^{-2}$ | 0 | $6.31\times10^{-13}$ | $1.58\times10^{-2}$ |
| pH 13.0 | $1\times10^{-1}$ | 0 | $1\times10^{-13}$ | $1\times10^{-1}$ |

Table 4.1: Calculated concentration of ions in the solutions at the measured pH, assuming the change of the water concentration is negligible, i.e. $[H_2O]\approx 55.4$ M . All concentration units are Molar. For $Na^+$ and $Cl^-$, the deviation from 1 M is tabulated.

10 eV of the absorption edge [95, 96] and would thus not affect the white line intensity as obtained by integration between 1070 eV and 1100 eV. Peak D is located at the transition to the EXAFS region in the absorption spectrum, where structural information on nearest neighbor distances and occupation numbers are convoluted with electronic structure information. [18] Here, the focus will be on the electronic structure information in the NEXAFS region.

While the white line intensity changes only marginally between pH 1.9 and pH 12.2, it is drastically reduced when going from the neutral solution to pH 13.0. The relative concentration of $Cl^-$ to $Na^+$ changes only marginally as a function of pH while the concentrations of $H^+$ and $OH^-$ change by orders of magnitude relative to the $Na^+$ concentration. Consequently, the observed changes in the NEXAFS spectra at pH 13.0 as compared to less basic pH can only be attributed to the presence of the hydroxide ions. In particular with respect to a quantitative analysis, the observed changes between pH 1.9 and pH 12.2 are too small to be interpreted. Our estimate of the intensity error which is dominated by potential systematic or non-linear changes in the absorption background is indicated in the figure by an error bar. In the following, the focus will be on the unambiguous effect at pH 13.0.

As a starting point for the discussion of the experimental findings, a local picture of solvated $Na^+$ ions will be used. As evident from table 4.1, only one hydroxide ion per 11 sodium ions is present at pH 13.0, while no significant amount of hydroxide or hydronium ions are present at pH 7. Neutral NaCl solu-

tions are typically modeled with sixfold water coordination of the $Na^+$ ion , as this coordination has been reported in a variety of experimental and theoretical studies. [66, 67, 82]. In the most simplistic scenario, one water molecule may be replaced by a hydroxide anion in a basic solution. In this fractionation model, the sodium ions would thus be either unaffected by the presence of hydroxide (hydronium) ions and still coordinated with an average of six water molecules, or they would have a hydroxide ion in their vicinity such that their electronic structure is influenced as compared to pure water coordination. With increasing $OH^-$ to $Na^+$ ratio, more $Na^+$ ions will be in the affected fraction; multiple occupancy of the $Na^+$ hydroxide can in first approximation be excluded on the grounds of the relative concentrations and the unfavorable electrostatic situation.

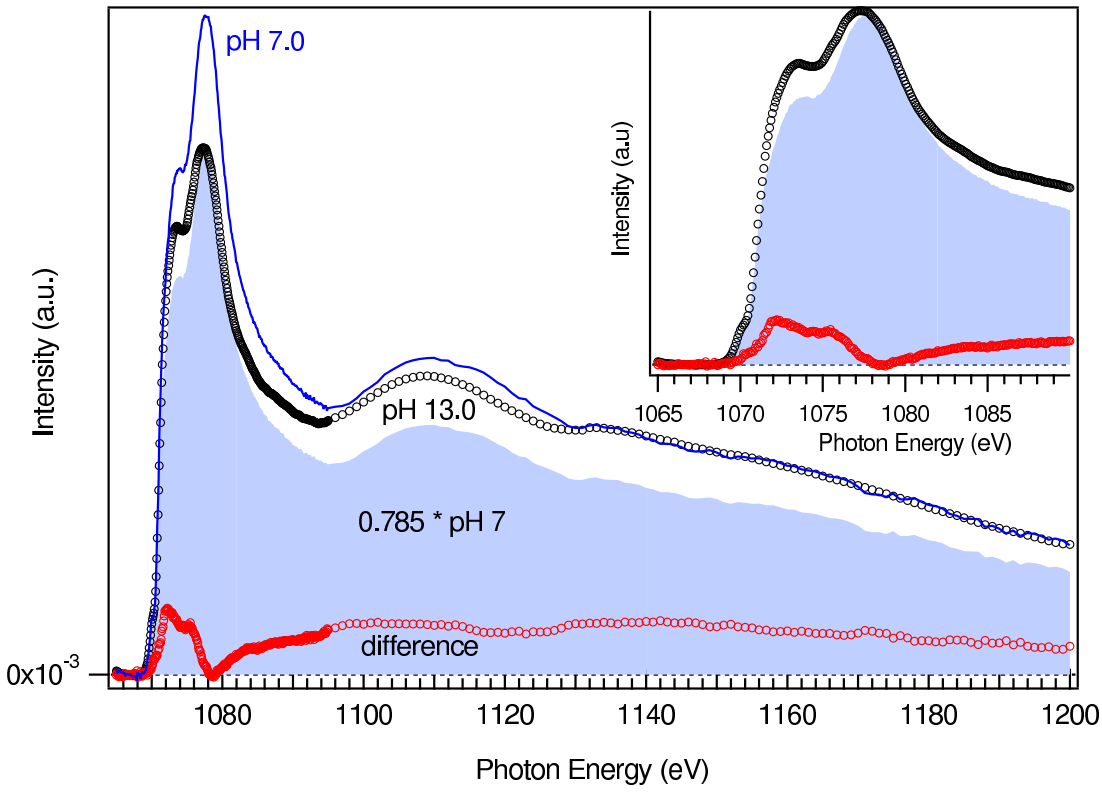


Figure 4.13: At most 78.5% of the pH ≅ 7.0 NEXAFS spectrum (blue line) can be subtracted from the pH ≅ 13.0 NEXAFS spectrum (black markers) while keeping the difference (red markers) non-negative. A magnification of the immediate near edge region is shown in the inset.

On this basis, the NEXAFS spectrum at pH 13 is expected to be a super-

position of two contributions: (i) a "pH 7-like fraction" where the $Na^+$ have the same local environment and the same electronic structure as at pH 7. This contribution should have a relative weight of $10/11 \approx 91\%$. (ii) an 'affected fraction' which is non-pH 7-like and which contains all $Na^+$ ions which have a local environment different from NaCl*aq at pH 7. The relative weight of this contribution should be $1/11 \approx 9\%$. This argument is simply based on the relative abundance of $H_3O^+$ or $OH^-$ relative to $Na^+$ ions as listed in Table 4.1. In this picture, it should be able to subtract 91% of the NEXAFS spectrum at pH 7.0 from the spectrum at pH 13.0. Obviously, much larger effect in the spectrum at pH 13 is observed. In Fig. 4.13 it is demonstrated that one can only subtract 78.5% of the pH 7 NEXAFS spectrum without obtaining an unphysical, negative intensity for the remaining fraction. Without any knowledge or assumptions on the spectral shape of the "affected fraction", this implies that *at least* 21.5% of the sodium ions in the solution are affected in their electronic structure by the presence of the hydroxide ions. Note that the existence of a variety of local configurations around the $Na^+$ ions in the spatial and temporal ensemble average is taken care of by the fact that measured data at pH 7 has been subtracted, which does reflect this ensemble average. As it is not known the spectral shape of the affected fraction *a priori*, the number of 21% affected $Na^+$ ions is a *lower* boundary for this value.

The fact that one can only subtract much less 'unaffected', pH 7-like intensity from the spectra at basic pH than one would expect from the $Na^+$ to $OH^-$ concentration ratios according to Table 4.1 clearly proves that more than one $Na^+$ ion is affected in its local electronic structure by a single $OH^-$. One thus can not maintain a simple, local picture of the interaction of $OH^-$ with $Na^+$ in the aqueous solution. The *minimum* number $N_{min}$ of $Na^+$ ions that are electronically affected by a *single* hydroxide at pH 13.0 is obtained from the values in Table 4.1 as

$$N_{min} = \frac{[Na^+]}{[OH^-]} \times (1 - f)$$

, where $f$=0.785 is the fraction determined by the subtraction procedure above. The minimum number of sodium ions affected by a single hydroxide ion determined in this way is $N_{min}$ =2.4±0.6. The relative error of 0.25 for this value is dominated by the intensity uncertainty as indicated by the error bar in Fig. 4.12, resulting in a relative error of 0.23. In comparison, the uncertainty in the pH value leads to a relative error of 0.07 (pH measurements differ by $\prec$0.04 pH before and after the x-ray experiment and the accuracy of the pH-meter callibration is estimated to be $< 0.05$ pH.) Furthermore, the $N_{min}$ value and

error are confirmed by an alternative data analysis procedure, where simply the ratio of the white line intensities at pH 7 and pH 13 are considered, neglecting shifts in peak positions.

For the basic pH region, one can therefore not maintain the simple picture of $Na^+$ ions, which are isolated by their solvation shells and interact only weakly by long range electrostatic forces. At the most extreme case in this study, for a 1 M NaCl solution at pH 13.0, one $OH^-$ is in interaction with at least 2.4 $Na^+$ ions. The interaction is so strong that it manifests itself in the local electronic states at the Na site, and such changes - certainly when they are as big as observed here - are generally discussed as the formation of ionic (or covalent) bonds between atoms. The duration of the x-ray transition at around 1080 eV can be roughly estimated as the time needed for one x-ray wavelength to pass by an atom; it is on the order of 4 $10^{-18}$ seconds. NEXAFS thus probes frozen configurations of a spatial ensemble, building up an ensemble average due to the spatial averaging and the temporal averaging required to record a spectrum. For pH 13.0, the data proves that one $OH^-$ interacts on average with 2.4 or more $Na^+$ ions at each moment in time. This requires a clustering of $Na^+$ around each $OH^-$. Alternatively, rather than having $Na_X^+OH^-(H_2O)_n$ entities with n≈5-6 and $N_{min}$ according to Fig. 4.13 , the data is also compatible with the existence of extended, percolated $Na^+$-$OH^-$ networks in the electrolyte at each moment in time. Although the minimum number of $Na^+$ ions affected by a single $OH^-$molecule can only be determined, the data suggest more pronounced networks or clusters at increased basicity.

To our knowledge no other experimental data exists that would allow conclusions about the existence of extended clusters or networks as described here. There are, however, several studies that are primarily concerned with the hydrogen network in water and electrolytes, which relate to some extent to the situation in this study. Structural studies by neutron scattering of aqueous NaOH solutions at high concentrations between 2 M and 18.5 M complemented by Car-Parinello-type molecular dynamics simulations report a concentration dependent number of water molecules in the $OH^-$ hydration shell and the existence of ion pairing at high ion concentrations. [97, 98] In spite of the different concentration regime studied, these results seem compatible with the findings of this study in that they find $Na^+$ $OH^-$ interaction, but they cannot serve as a test for the existence of networks or large clusters. Dynamical studies of the reorientation time of water molecules in bulk water vs. water molecules in the first solvation shell of various ions show that the dynamics outside the

first solvation shell is practically unaffected by the ions' presence. [99,100] These results on the majority species $H_2O$ are not in contradiction to the presence of spatially extended $Na^+$ $OH^-$ interaction, which could be envisioned to take place in a mainly unaffected matrix of hydrogen bonded water molecules. Molecular dynamics simulations for aqueous NaCl solutions (not as a function of pH) have found evidence of the formation of large clusters. Ion pairs, triplets and larger clusters associated with a dozen or more solvent molecules were predicted. [76]. Again, the role of pH and in particular of $OH^-$ has so far not been investigated.

The principle of increasing or decreasing the white line intensity for $Na^+$ upon pairing with hydronium or hydroxyl respectively can be theoretically demonstrated using the DFT technique (StoBe DeMon package) [12]. In Fig.4.14 the simulated NEXAFS spectra of Na k-edge are presented for three clusters models $[Na^+(H_2O)_6]$,$[Na^+(H_2O)_5OH^-]$, $[Na^+(H_2O)_5(H_3O)^+]$. Before calculating the NEXAFS spectra for these models, the geometry of these structures are optimized. The optimized models show that the hydroxyl ion tends to be at close interaction with $Na^+$ while the hydronium moves away. The geometry optimization is done by Gaussian03 [14], using the DFT method, B3LYP functional, and augmented double zeta basis set. The optimized output configurations have been used as an input for the StoBe simulation. The simulated spectra show a decrease of the white line under the K-edge of sodium upon pairing with the hydroxyl ion. On the other hand, the hydronium ion has negligible effect on the white line intensity since the ions move far away from each other. From this ab intio calculation one can not predict the type or the full geometrical structure of the cluster which is build between the sodium and the hydroxyl ions.

To get a better structural picture for the nature of the cluster between the sodium and the hydroxyl ion, a classical molecular dynamics simulation was carried out by Lukasz Cwiklik and Pavel Jungwirth from the Institute of Organic Chemistry and Biochemistry, Academy of Sciences of the Czech Republic. A system consisting of 110 water molecules with 11 $Na^+$, 10 $Cl^-$, and 1 $OH^-$ ion, has been analyzed (which corresponds to a 5 M concentration of NaCl at pH = 13). The concentration of 5 M was chosen to keep the total number of water molecules small enough for the system to be computationally feasible, while retaining the relative abundances between ions. A polarizable force field for water and ions was employed, with a slightly expanded (by less than 10 %) van der Waals radius of hydroxide in order to avoid the so called polarization catastrophe [101]. A relatively small system was chosen in order to have a single hydroxide anion

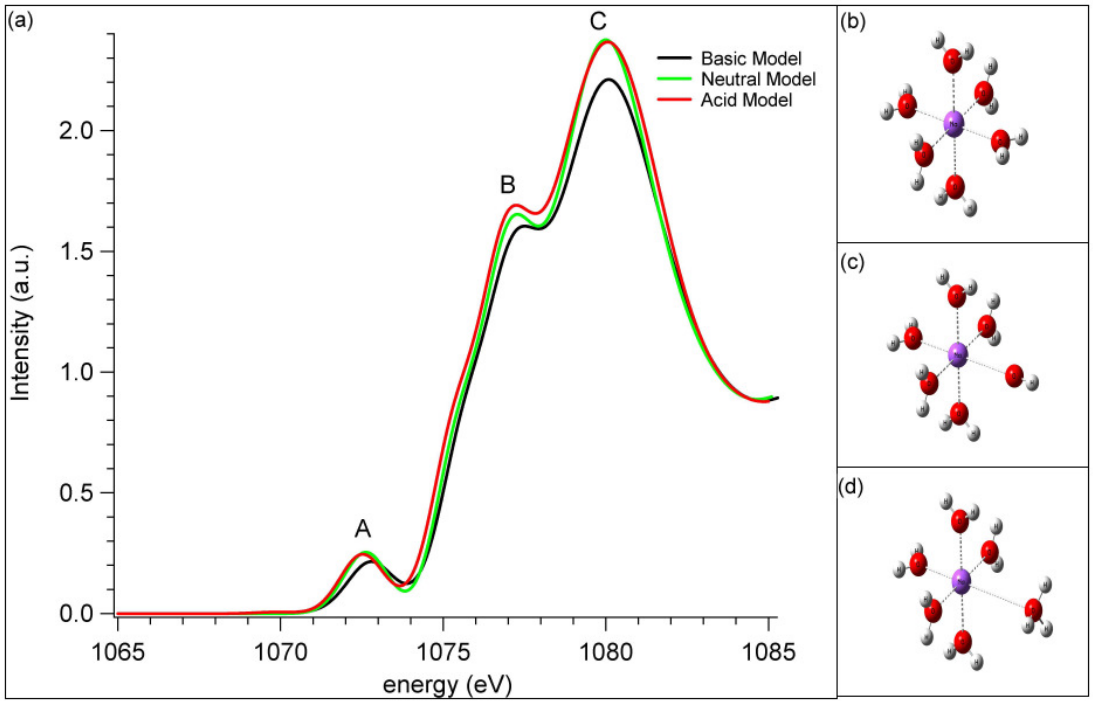


Figure 4.14: Optimized model cluster using Gaussian03 for (b) neutral model, (c) basic model, and (d) acid model. (a) Simulated NEXAFS spectra for Na K-edge using the acid (red), neutral (green) and the basic model (black) as presented on the top of the figure.

in the simulation box of 15x15x15 $\mathring{A}^3$, making thus the analysis of results more straightforward. Moreover, the classical force field is verified against ab initio molecular dynamics employing a BLYP functional for the same system. Within the ab initio approach only short trajectories (several picoseconds) are computationally feasible. These confirmed semi-quantitatively the conclusions below from statistically converged classical molecular dynamics simulations.

A bulk system was modeled applying 3D periodic boundary conditions and the Ewald summation method was employed to account for long range electrostatic interactions. After a sufficiently long equilibration within the (NPT) ensemble, the ensemble was changed to (NVT) at T = 300 K and a 2 ns trajectory was collected and analyzed. In Fig. 4.15 radial distribution functions between oxygen atom in $OH^-$ and $Na^+$, and between $Cl^-$ and $Na^+$ are presented together with the integrated curves. For distances below 6 $\mathring{A}$ a strong difference between hydroxide oxygen-sodium and chloride-sodium distributions can be seen.

The first peak for both curves corresponds to a contact ion pair. Such a pair is formed in both cases with the anion–cation distance being shorter for hydroxide compared to chloride (2.5 $\AA$ vs 2.8 $\AA$). Then, at the distance of about 4 $\AA$ there is a peak on the first curve corresponding to a second sodium cation in the vicinity of hydroxide and at 4.6 $\AA$ there is another peak correlating roughly with a third sodium cation. The integrated distribution shows that there are on average 3 sodium cations within 6 $\AA$ from the hydroxide oxygen. On the $Cl^- - Na^+$ curve there is no peak around 4 $\AA$. Instead there are two peaks at approximately 5 $\AA$, due to which the number of neighboring cations also reaches 3 at 6 $\AA$.

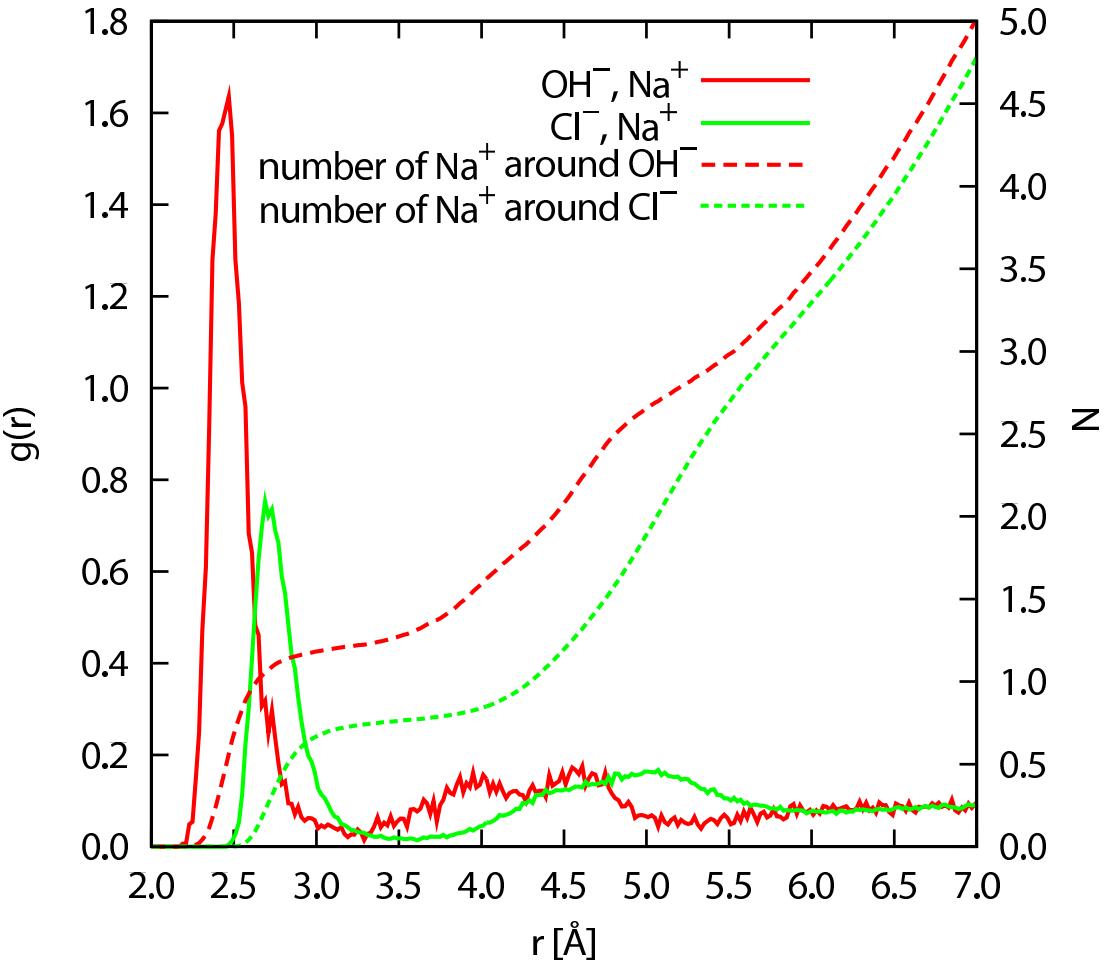


Figure 4.15: Hydroxide oxygen-sodium and chloride-sodium radial distribution functions and the corresponding integrated curves, which give the number of cations within a given distance from the anion.

In Fig.4.16 density plots for atoms and ions around the hydroxide are presented. Projections of three-dimensional maps for two different isovalues are presented. For sodium cations, three regions around $OH^-$ can be identified. The first density maximum of sodium (M1), located 2.5 $\AA$ from oxygen opposite to the hydrogen of $OH^-$ can be interpreted as a contact ion pair. The second sodium maximum (M2) appears on the hydrogen side of hydroxide, while the third one (M3) is on the oxygen side behind the first maximum. The latter two maxima, roughly corresponding to the second and third sodium cation, represent solvent-separated ion pairs, as is evident from the overlap of the sodium and water isosurfaces in Fig.4.16). A plot for an increased density isovalue of Fig.4.16.2b visualizes the delocalization and the three sodium cations can now be seen to form a structured cluster around $OH^-$ whereas more distant cations are homogeneously spread around the hydroxide.

The molecular dynamics simulations allow us to conclude that ordered local structures of the hydroxide anion and, on average, $\approx 3$ sodium cations exist in the simulated mixed solution, similarly as in pure concentrated NaOH aqueous solutions. [102] One cation forms a contact ion-pair and at least the two next nearest sodium ions are interacting with the hydroxide ion as solvent separated ion-pairs.

While the molecular dynamics simulation represents the $Na^+$ / $OH^-$ /$Cl^-$ ratios of the experiment correctly, it overestimates the ion concentrations relative to the solvent by a factor of five. At 1 M concentration one might thus expect a generally reduced number of contact ion pairs. However, theoretical results for NaCl solutions [103] show that going from 4.4 M to $\approx$ 0 M concentration the average number of water molecules in the first solvation sphere for $Na^+$ increases only by 5% and the structure of $Na^+$-$Cl^-$ radial distribution is unaffected. For NaOH in aqueous solution it was reported that the changes in coordination number of Na-OH with concentration are negligible. [102] Thus one can expect from the theoretical results to approximate the experimental situation reasonably well.

The results from the molecular dynamics simulation, namely that on average 3 sodium cations are found within a 6 $\AA$ sphere around a $OH^-$ ion and that one of them is forming a contact ion-pair is in good agreement with the experimental observation that a single $OH^-$ affects 2.4$\pm$0.6 $Na^+$ ions with respect to their electronic structure. In the light of the theoretical findings, one expects the sodium ion forming a contact ion-pair (M1 in Fig. 4.16) to have a strongly altered electronic structure as compared to a purely water coordinated $Na^+$, while the sodium ions M2 and M3 in solvent-separated ion-pairs can be expected to be

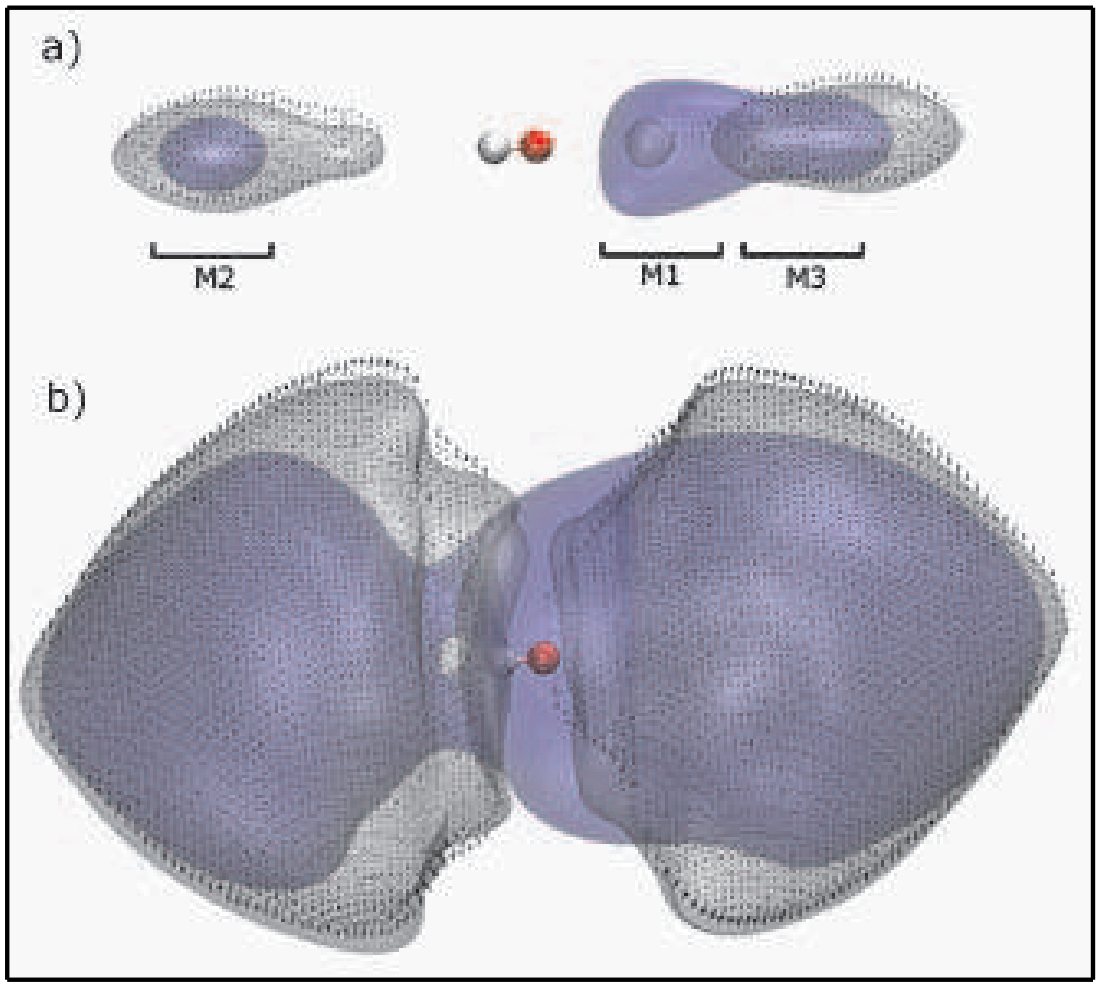


Figure 4.16: Isosurfaces of sodium and water densities around a hydroxide anion for (a) density isovalues of 1.9 for water and 4.2 for sodium and (b) density isovalues of 4.0 for water and 6.0 for sodium. Color coding: red oxygen, white hydrogen, blue sodium, gray water oxygen, and black dots water hydrogen. The first three maxima (M1, M2, M3) for sodium are shown in (a).

affected to a lesser degree. While the existence of a local clustering as inferred from the experiment could be corrobated by the molecular dynamics simulation, it is not possible to check if chains or even percolated $Na^+$–$OH^-$ networks exist in the liquid. Such a phenomenon would be compatible with the experimental data, and it would imply an influence on the hydrogen bond network in the bulk of the electrolyte solution. We expect that this question can be addressed in the future by molecular dynamics calculations with a significantly increased unit cell.

### 4.3.3 Conclusion

We have presented experimental and theoretical results on the electronic structure and the local geometry of the ions and solvent molecules of aqueous NaCl solution as a function of pH. For pH 13, a clear change of the local electronic structure at the sodium ions as compared to more acidic solutions is observed. From the experimental data, we conclude that one $OH^-$ at pH 13 interacts on average with at least 2.4±0.6 $Na^+$ ions in the spatio-temporal ensemble average. This finding is in agreement with the results from our molecular dynamics simulations, namely that on average three sodium cations are found within a 6 Å sphere around a $OH^-$ ion and that one of them is forming a contact ion pair. In the light of the theoretical findings, we expect the sodium ion forming a contact ion pair (M1 in Fig. 4.16) to have a strongly altered electronic structure as compared to a purely water coordinated $Na^+$, while the sodium ions M2 and M3 in solvent-separated ion pairs can be expected to be affected to a lesser degree. Concerning extended ion organization in solution, MD simulations show a remarkable ability of $OH^-$ to form oriented, roughly collinear anion-cation structures. This distinguishes the present system from simple salt solutions (such as aqueous NaCl), where sperical ions at best pair to form on average isotropic clusters at high concentrations.

## 4.4 Solvent versus Non-Solvent Shared Ion-Pairs in $NiCl_2$ Solution

Part of this section published in *JOURNAL OF PHYSICAL CHEMISTRY B 111, 4440 (2007)*

### 4.4.1 Introduction

Most properties of transition-metal ion electrolyte solutions depend on the ability of solvent and solute to interact, and hence on the nature of the complex ion formation. One important property is the Gibbs free energy of solvation which requires an assumption on the effective ionic radii $R_{ion}^{eff}$ which is often expressed by $R_{ion} + \Delta R$. Here, $\Delta R$ is a function taking into account the first hydration shell [104]. Several methods have been used to probe the local geometrical structure of transition metal ions in solution experimentally. In an x-ray diffraction study of saturated $NiCl_2$ solutions, Waizumi et al. have reported the existence of mixed-ligand chloroaqua octahedral complexes in addition to sixfold water coordinated Ni ions, i.e. the existence of direct contact ion pairs [105]. A detailed picture for ion clustering in solution, including the solvent-shared hydration shell, has been given by Fulton et al [92]. Based on their combined X-ray Absorption Near Edge Structure (XANES) and EXAFS studies, these authors have suggested a long-range interaction between ions in the solution which leads to a solvent-shared ion-pair. Direct contact ion-pairs between the cations and the anions have been argued to be negligible in many cases even at high concentration. This is in agreement with a neutron diffraction study by Badyal et al. [93], also providing evidence for the existence of solvent-shared ion-pairs.

For $Ni^{2+}$ in aqueous solution, neutron diffraction studies [106, 107] as well as x-ray diffraction [105] have shown that $Ni^{2+}$ has a coordination sphere of six water molecules. Inner sphere contact pairs of Ni-Cl have been suggested to exist for 8% of the Ni ions in a x-ray diffraction study of 3 M $NiCl_2$ aqueous solution [108]. X-ray diffraction of $NiBr_2$ aqueous solution has shown strong experimental evidence for ion-pair formation at 2 M concentration within octahydration geometry. [109]. Here we study the range form diluted (50 mM) to concentrated (1.5 M) aqueous $NiCl_2$ solutions, where we expect a transition in the importance of interionic interactions.

In this section we present NEXAFS spectra for the $Ni^{2+}$ L-edge in aqueous

$NiCl_2$ electrolyte solution as a function of the concentration, starting from the solid $NiCl_2$. Two distinctive spectral features can be assigned as fingerprints of direct contact ion-pairs and solvent-shared ion-pairs in the solution. The spectra have been analyzed by the means of a charge transfer multiplet simulation [56, 57, 69]. The multiplet approach has been extensively used in the analysis of L-edge spectra of transition metals, where it is established as a method for probing the metal ligand charge transfer [70–73]. Moreover, in order to shed more light on these electronic as well as geometric changes, two additional experimental techniques are combined in this study investigating the behavior of $NiCl_2$ salt dissolved in water. Resonant inelastic x-ray scattering (RIXS) at the $L_3$ edge of Ni is used to study the electronic structure. Extended x-ray absorption fine structure (EXAFS) is used to investigate the change in the local geometrical structure around the $Ni^{2+}$ ions in the same system. EXAFS spectra are modeled using FEFF8 program package [56, 57, 74] [FEFF has been discussed in Section 2.2.4].

### 4.4.2 Results and Discussion

#### NEXAFS

In Fig.4.17, the $Ni^{2+}$ L-edge electron yield NEXAFS spectrum for $NiCl_2.6H_2O$ hydrated solid is presented as a reference for the liquid measurements. The 2p (L-edge) NEXAFS spectrum of $Ni^{2+}$ has a number of peaks that split into two main regions, one at 852 eV and one at 870 eV. The structures around 852 eV are related to the $L_3$ edge (P1 and P2 peaks). The features around 870 eV are related to the $L_2$ edge (P4 and P5 peaks); the 2p spin-orbit coupling leads to a splitting of approximately 18 eV. Peak P1 and peak P4 relate to a $2p^5 3d^9$ final state of triplet character, i.e. where the spins of the 2p shell and 3d electron are parallel. In contrast, peaks P2 and P5 relate to a singlet final state. A satellite peak above the $L_3$ edge at around 858 eV appears for the solid $Ni^{2+}$ (P3 peak) The spectrum agrees well with published data by Laan et al [110]. Within the $L_3$-edge, two peaks P1 and P2 split by 1.6 eV are observed. The satellite peak is known to be due to the Ligand Metal Charge Transfer (LMCT) from $Cl^-$ to $Ni^{2+}$ [69], which is possible due to the close proximity of Ni and Cl in the solid. An overview spectrum for $NiCl_2$ aqueous solution is shown for comparison. As for all liquid spectra, NEXAFS was measured by the fluorescence yield (FY). The changes in the peak intensities and splittings will be discussed as a function of concentration in the context of Fig.4.18

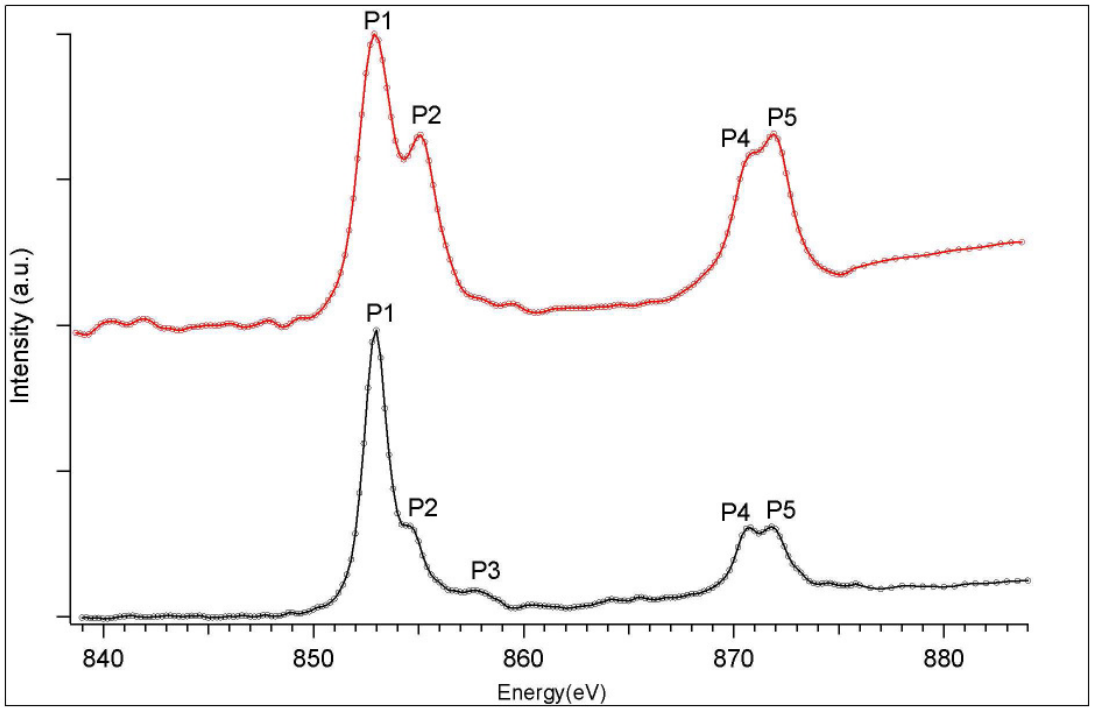


Figure 4.17: Nickel L-edge EY-NEXAFS spectrum for solid $NiCl_2$ (black), and FY-NEXAFS for $NiCl_2$ 1500 mM (red).

As a function of electrolyte concentration from 50 mM to 1500 mM, a systematic change in the NEXAFS spectral features is observed as seen in Fig.4.18. Even at the highest concentration investigated, peak P3 is not detectable against the background noise level in the spectra of the electrolytes. The absence of this peak compared to the solid reflects the non-existing or at least strongly reduced amount of direct interaction between $Ni^{2+}$ and $Cl^-$ in the electrolyte solution as compared to the solid. However, given the slight uncertainty in the baseline, our results would still be consistent with 8% of Ni atoms in direct-contact pairs with $Cl^-$, as reported for 3 M $NiCl_2$ solution. [108] As a second important difference between bulk and electrolyte spectra, the energy splitting within the $L_3$ edge in the electrolyte solutions is 2.4 eV compared to 1.6 eV for the solid. This increase of the $L_3$ splitting energy can be assigned to the absence of direct contact ion-pairs as well, as it will be discussed later.

The most prominent intensity change is the increasing P2/P1 intensity ratio for increasing $NiCl_2$ concentration in the solvent. For geometrical reasons, FY-NEXAFS spectra can exhibit distorted intensities if the edge absorption of

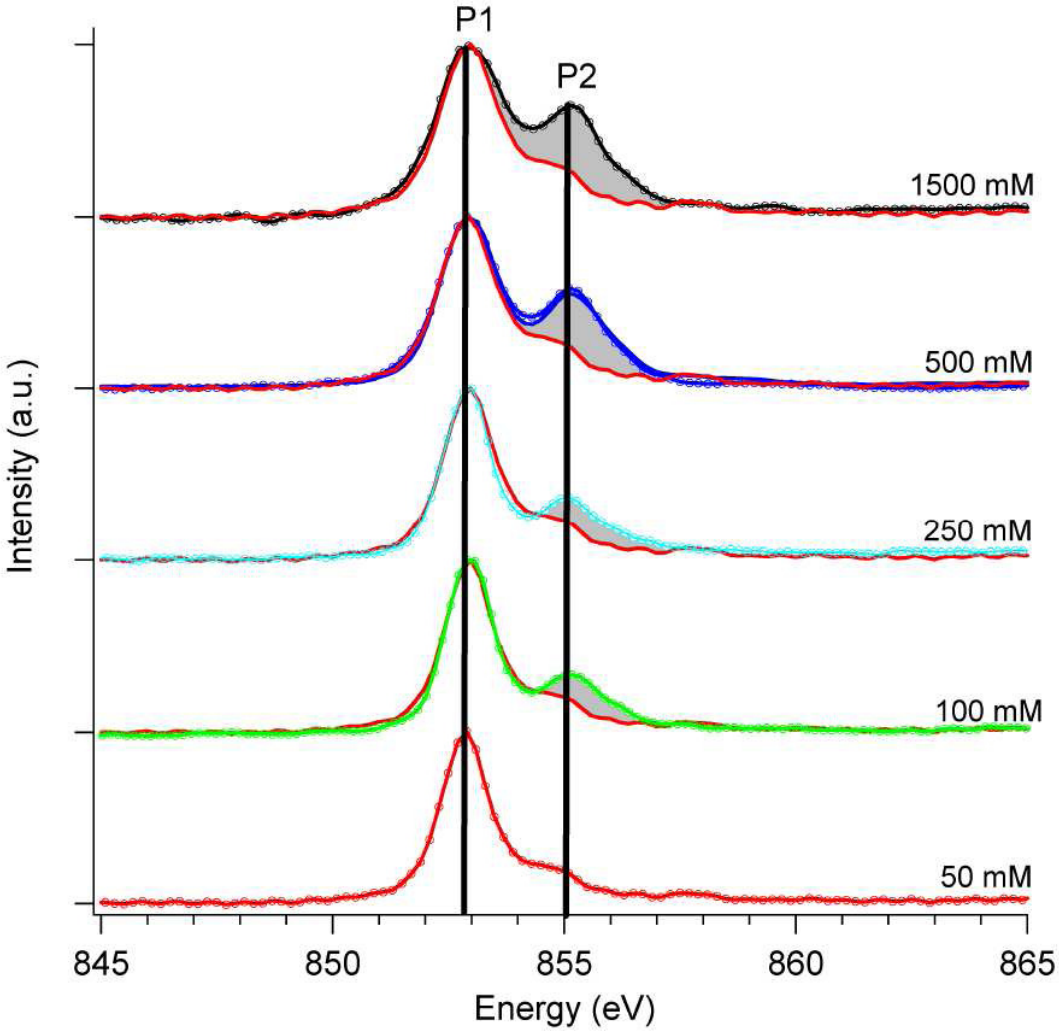


Figure 4.18: Nickel $L_3$-edge FY-NEXAFS spectra for $NiCl_2$ solution as a function of the concentration. For comparison, the 500 mM sample spectrum (blue) was measured in the static cell (line with circles), and in the liquid flow jet (solid line). A simulation of the saturation effect due to the fluorescence detection mode is presented under each spectrum (red solid line), the difference to the experimental data at the P2 peak has been shaded. If the electronic structure would *not* change with concentration, the FY-NEXAFS spectra would appear like the simulated spectra. This effect is geometrical in nature and solely due to the influence of saturation.

interest is larger than the background absorption [23, 25]. This effect becomes important in concentrated samples, and will be strong in solid $NiCl_2$. For the

solid, NEXAFS in electron yield (EY) mode is used to measure the absorption cross section (Fig.4.17), which due to its surface sensitivity does not suffer from these distortions. This approach is not feasible for the liquid samples. Here, the concentration-dependent saturation effect is quantified. Based on the atomic absorption cross-sections the distortion is found to be negligible for 50 mM $NiCl_2$ solution. Based on this absorption cross-section, we calculate how geometric saturation effects would distort the spectra at higher concentration [23, 25]. These simulated spectra are presented in Fig.4.18 along with the measured spectra for different electrolyte concentrations.

Clearly, this geometrical saturation effect alone can not account for the observed intensity changes as a function of electrolyte concentration. It is the remaining effect of concentration on the NEXAFS spectra which will be discussed in detail in this section. It is evident from the NEXAFS spectra that the electronic structure locally at the $Ni^{2+}$ atoms in the solution changes as a function of electrolyte concentration. The change is such that peak P2 increases relative to P1 for increasing electrolyte concentration. Furthermore, a change in multiplet splitting energy was observed between solid and liquid spectra. In the following, these changes in the electronic structure will be rationalized on the basis of electronic structure calculations, where symmetry parameters are being varied.

In an NEXAFS experiment, a spatial ensemble average over temporally frozen configurations is observed. Rigorously, such a system should be described by an ensemble average over a multitude of different local $Ni^{2+}$ environments in the liquid, obtained e.g. by molecular dynamics simulations. Here, a much simpler route will be followed trying to qualitatively understand the observed spectral changes analyzing one model. In order to simulate the observed spectral changes, multiplet calculations were performed, where $Ni^{2+}$ in an $O_h$ symmetric crystal field is considered. This approach is justified by the fact that the highly directed Ni d-orbitals favor a quite rigid local symmetry, as known from complex chemistry. For highly concentrated $NiCl_2$ solutions, local structural data was well described in $O_h$ symmetry, [105] as expected for $Ni^{2+}$ with a $d^8$ electron configuration.

In Fig.4.19 the simulated spectra obtained using a crystal field of 1.1 eV for the $d^8$ configuration, and a $d^9\underline{L}$ charge transfer state was included in order to describe the electron transfer from $Cl^-$ to the valence d-orbitals of $Ni^{2+}$. This configuration interaction with a contribution of the $d^9\underline{L}$ configuration of about 14% can explain the appearance of the P3 peak in the experimental spectra.

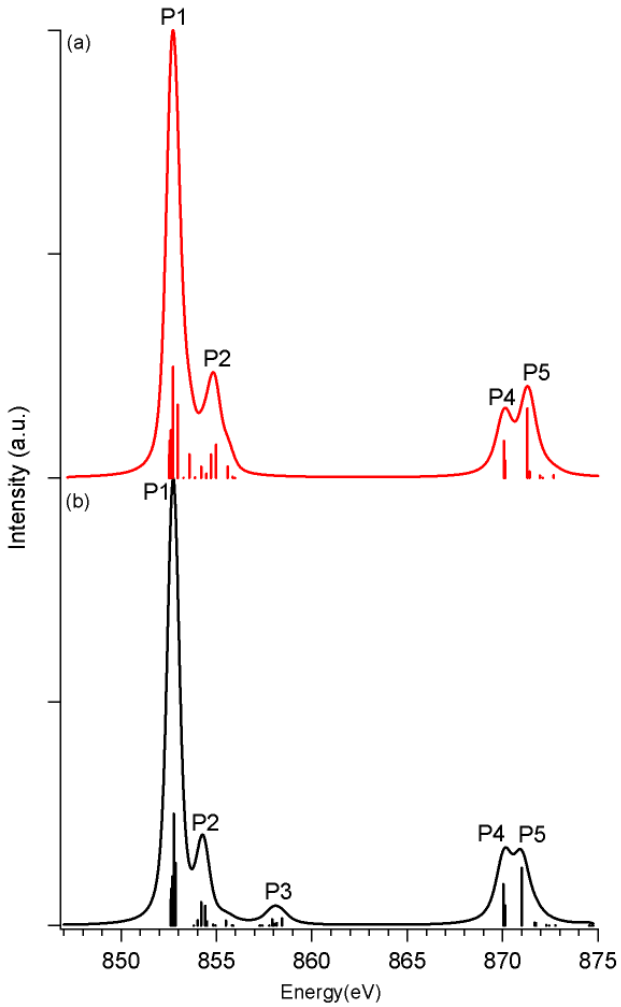


Figure 4.19: Calculated $Ni^{2+}$ L-edge NEXAFS spectra using 1.1 eV crystal field. (a) For pure $d^8$ configuration, (b) For 86% $d^8$ configuration mixed 14% $d^9\underline{L}$ configuration. Calculated states are indicated by sticks and have been broadened by 0.25 eV and 0.3 lorentzian.

This $d^9\underline{L}$ charge transfer can only be significant with $Ni^{2+}$ and $Cl^-$ being in direct contact, as in the solid $NiCl_2$. The significant reduction of the P3 peak intensity upon dissolving the solid $NiCl_2$ in water is consequently explained by the absence of $d^9\underline{L}$ charge transfer; that is, the $Cl^-$ ions have moved out of $Ni^{2+}$ in the first hydration shell. Furthermore, this treatment reproduces the experimentally observed P1-P2 peak energy splitting which is 1.6 eV for solid $NiCl_2$ and 2.4 eV for the solution. The simulated spectra have peak separations of 1.65 eV for mixed $d^8$ with $d^9\underline{L}$ configurations and 2.3 eV for a pure $d^8$

configuration. This implies that the ions in solution have rather weak charge transfer, since charge transfer compresses the multiplet splitting. The simulated spectra in Fig.4.19 reproduce the experimental NEXAFS spectra for the solid $NiCl_2$ well, including the spectral finger print (P3) for the existence of ion-pairs. Within pure $O_h$ calculations, the change of the P2/P1 peak ratio in the salt solutions as a function of concentration (Fig.4.18) can not be reproduced. Only the most dilute 50 mM $Ni^{2+}$ solution can be described in perfect $O_h$ symmetry with a pure $d^8$ configuration.

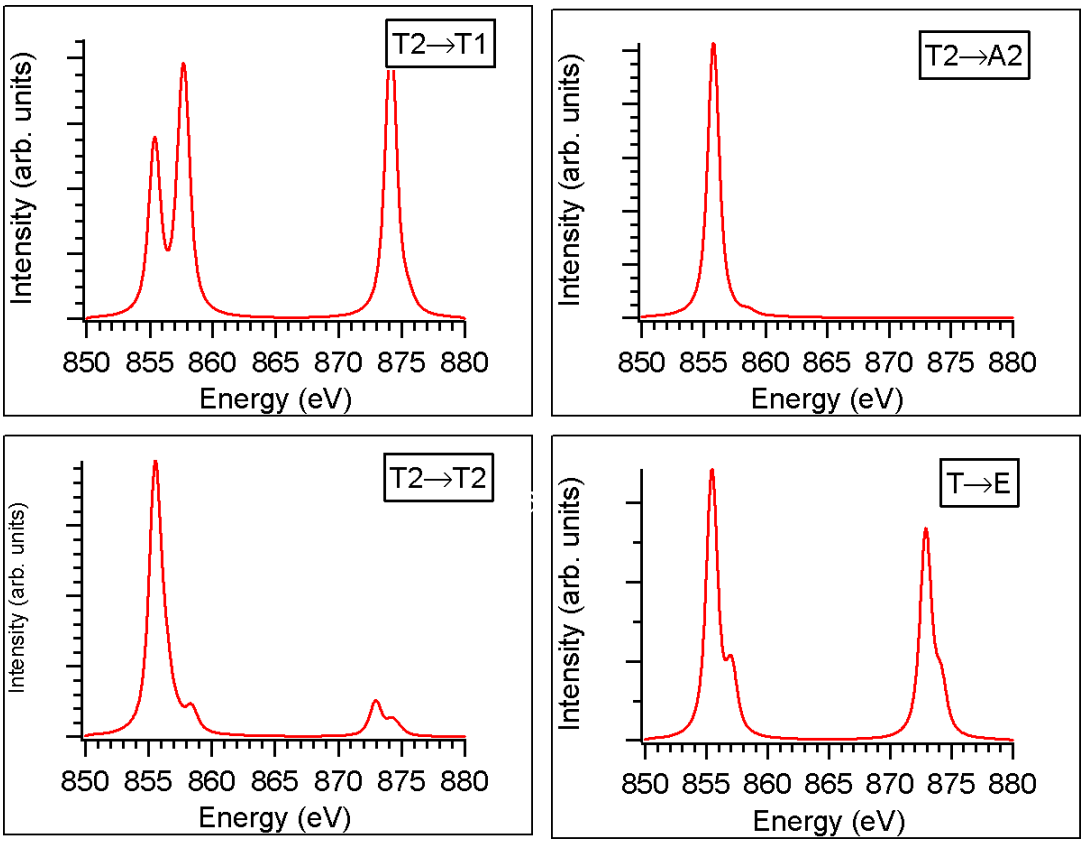


Figure 4.20: Calculated $Ni^{2+}$ L-edge NEXAFS spectra using 1.1 eV crystal field for the different transition matrix contributions.

In order to explain the change of the fluorescence yield as a function of $Ni^{2+}$ concentration, one has to highlight the fact that the calculated absorption for $d^8$ configuration in an $O_h$ crystal field consist of four dipole matrix element components e.g. $\langle f|p|i\rangle = \alpha \times \langle T_2|T_1|T_1\rangle + \beta \times \langle T_2|T_1|A_2\rangle + \gamma \times \langle T_2|T_1|T_2\rangle + \delta \times \langle T2|T_1|E\rangle$, where $\alpha$, $\beta$, $\gamma$, and *delta* are $= 1$. The contributing spectral

part of each matrix element is presented in Fig.4.20. We observe that in order to reproduce the experimental NEXAFS spectra for $Ni^{2+}$ solution as a function of concentration, these four matrix elements are added not equally. Further analysis shows that the main channels for the singlet states (855 eV, 872 eV) have $T_1$ character, while the triplet $2p^5 3d^9$ states (853 eV,870 eV) have mixed $T_2$, E and $A_2$ character. This implies that one can simulate the variation in triplet (P1 peak) versus singlet (P2 peak) states by varying the ratio of the different coefficients $\alpha$ through $\delta$, and in particular by varying $\alpha$ with respect to the remaining coefficients.

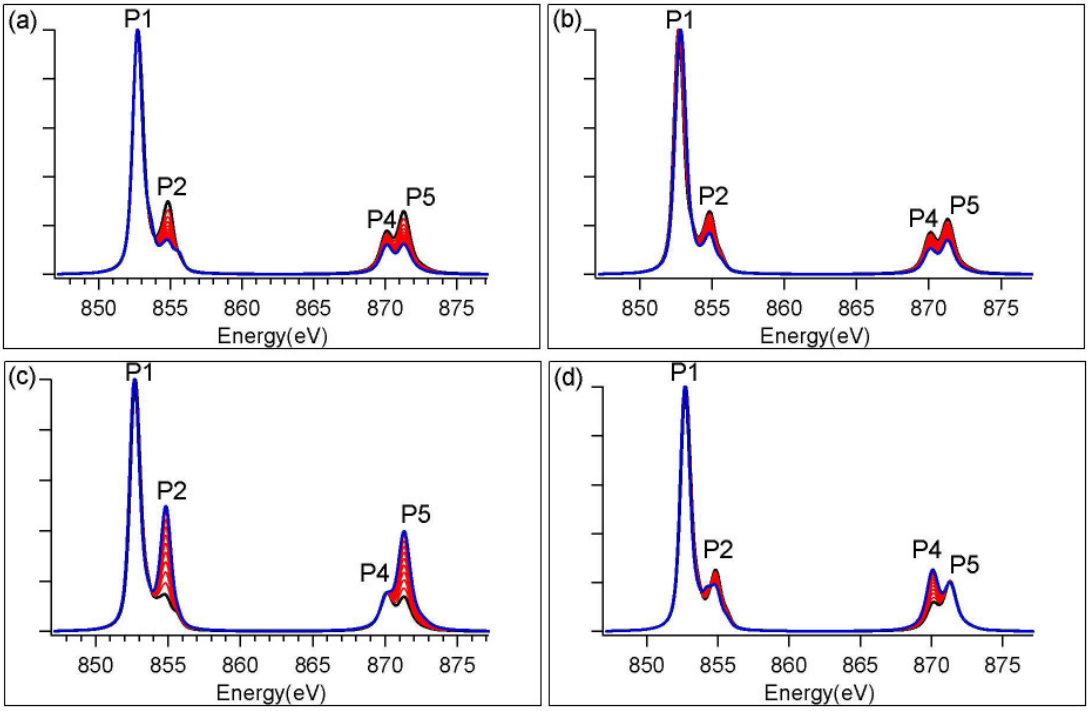


Figure 4.21: Hypothetical $Ni^{2+}$ $L_3$-edge NEXAFS spectral shape upon variation of the different transition matrix contributions. Spectra are calculated for a crystal field of 1.1 eV and pure $d^8$ configuration. The relative weight of (a) $\alpha$, (b) $\beta$, (c) $\gamma$, (d) $\delta$ has been varied from 0.5 (black) to 3 (blue). The resulting spectra have been normalized on the P1 peak.

In Fig. 4.21, the resulting variation of the spectral shape of the coefficients $\alpha$ through $\delta$ is plotted, within limits such that the overall spectral shape starts to become unphysical for the extreme values of $\alpha$ and $\gamma$. This defines a variation interval from 0.5 to 3.0, outside this interval the overall intensity ratio of

$L_3$-related vs. $L_2$-related peaks is clearly disagreeing with the experimental spectra in the literature and in this work. Over this parameter interval, both the $\langle T_2|T_1|T_1\rangle$ and $\langle T_2|T_2|T_1\rangle$ matrix elements show a strong variation of the P2/P1 intensity ratio, with an inverted sign of the intensity ratio dependence on $\alpha$ and $\gamma$, respectively. A variation of $\alpha$ from 3.0 to 0.5 while keeping the other coefficients constant at 1.0 does reproduce the variation in spectral shape that is observed experimentally, i.e. it increases the P2/P1 peak intensity ratio. Consequently, linear combinations with variation of all four coefficients can generate theoretical spectra which describe the experimental findings as a function of electrolyte concentration well. The change of the relative contributions of the $\langle T_2|T_1|T_1\rangle$ matrix elements to the total transition probability reflects a changing weight of the spectral contribution of the triplet state versus the singlet state. The fact that the experimentally observed changes in the $Ni^{2+}$ L NEXAFS spectra can be explained by this procedure suggests that the change of the singlet/triplet ratio may be the most significant change of the electronic structure at the $Ni^{2+}$ site induced by the increase of the ion concentration in the electrolyte.

This interpretation is based on experimental electronic structure NEXAFS data in comparison to the multiplet calculations of the spectral shape in $O_h$ symmetry and with distortions, which one would encounter e.g.; if the crystal field strength on one high-symmetry axis would be changed relative to the two remaining high-symmetry axes. The theory does not rely on particular structural models of the ions and solvent molecules in the electrolyte beyond symmetry arguments. From an atomistic point of view, one would expect reduced interionic correlation lengths for increasing electrolyte concentration. When approaching a saturated aqueous $NiCl_2$ solution (4.6 M at RT), one might expect to find evidence of direct contact $Ni^{2+}$ $Cl^-$ ion pairs, as reported by Waizumi et al. [105]. Even at 1.5 M concentration, no appreciable weight is found for direct contact ion pairs as evidenced by the lack of intensity at the P3 peak position. This leads to conclude that the changes in the local electronic structure at the Ni site as a function of electrolyte concentration must be due to indirect, solvent-shared, ion-pair (or ion cluster) formation. In a simple picture one could describe these findings as evidence of local distortions due to indirect ion-pairs, with increasing distortion for increasing ion concentration in the electrolyte. These distortions manifest themselves in the ensemble average of quasi-frozen configurations during the x-ray absorption interaction time via the multiplet field experienced by the $Ni^{2+}$ ion. The next lower symmetry which might be produced upon distorting the $O_h$ symmetry around the $Ni^{2+}$ is $D_{4h}$. In this symmetry point group, the $t_{2g}$ symmetry states in the $O_h$ split into $e_g$

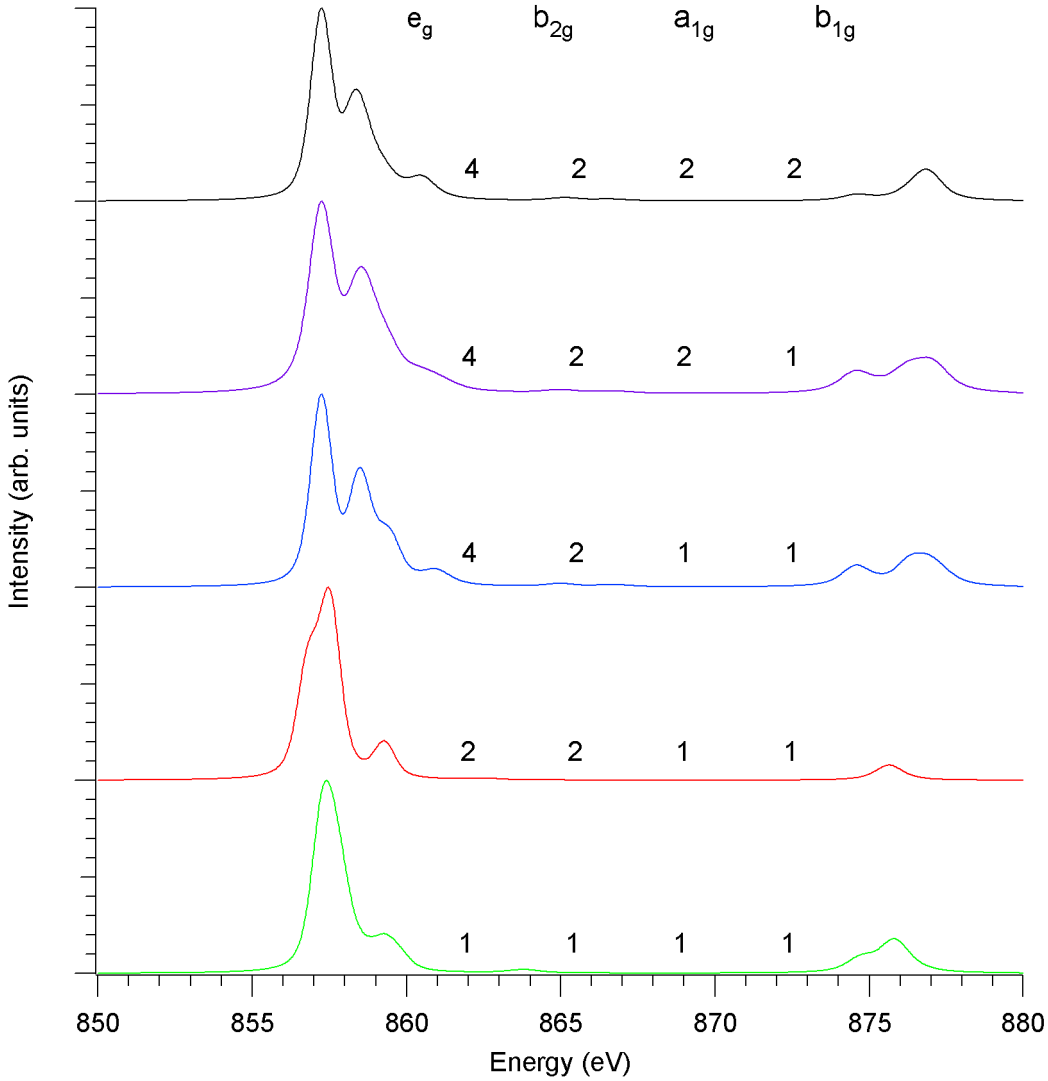


Figure 4.22: Simulated $Ni^{2+}$ L-edge FY-NEXAFS spectra in $d_{4h}$ symmetry upon varying the weight for each symmetry states. The number on each spectra present the relative contribution from each state, as highlighted on the top of the figure.

and $b_{2g}$, and the $e_g$ symmetry state in the $O_h$ split into $a_{1g}$, and $e_g$ in $d_{4h}$ crystal field. In Fig.4.22, calculated spectra for $Ni^{2+}$ using $D_{4h}$ symmetry group are presented. The weight for each symmetry state has been varied, which imposes further distortion to the $D_{4h}$ symmetry. Neither the simulated spectrum from the pure $D_{4h}$ symmetry group, nor from the distorted ones could reproduce the experimental spectra for $Ni^{2+}$ ions in solution. From this simulation, one can argue that increasing the strength for the solvent-shared ion-pair in

solution induces a slight distortion in the $O_h$ field around the $Ni^{2+}$ ions. This distortion was not significant in the way to change the $O_h$ local symmetry to lower symmetry like $D_{4h}$. Furthermore, this can be theoretically reproduced upon varying the weight of the transition dipole matrix elements for the $O_h$ field. The concept of solvent-shared ion-pairs is in line with EXAFS and neutron diffraction studies, where a long range arrangement of oppositely charged ions in solution via shared solvation shells was observed [92, 93].

### RIXS

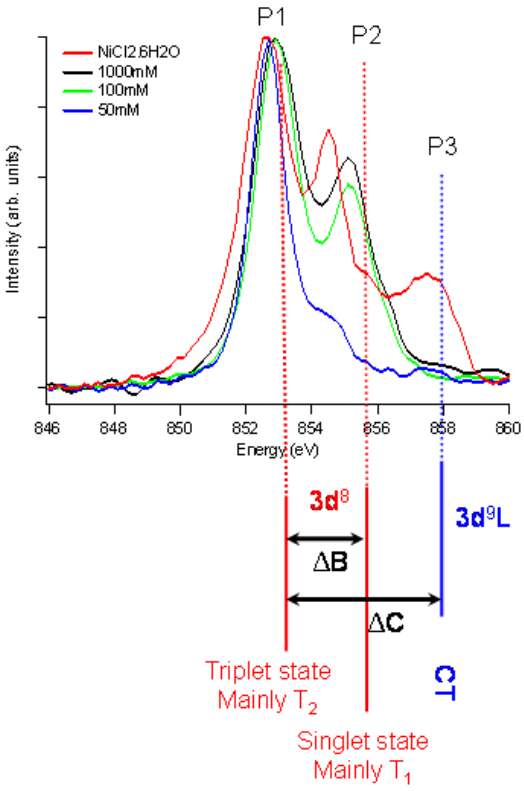


Figure 4.23: (a) Nickel $L_3$-edge FY-NEXAFS spectrum from $Ni^{2+}$ hydrated solid and solution. Energy diagram for the origin of each state under each peak are presented at the right of the spectra.

RIXS spectra from $NiCl_2$ electrolyte solution are presented in Fig.4.24 as a function of concentration. Excitation energy was 852.5 eV corresponding to the first excitation energy of the $L_3$ absorption feature. The emission spectrum

of the solution has been compared to the spectra obtained from the powder form. The origin of the emission spectra can be explained with the NEXAFS spectra presented in Fig.4.23. As was shown in the previous section 4.4.2, the first NEXAFS peak is caused by the excited triplet state, the second peak is caused by the excited singlet state, and the third peak can be assigned to the charge transfer feature. For the $NiCl_2$ powder, excitation into the first absorption maximum is followed by relaxation from the singlet (peak B in emission) as well as from the charge transfer state CT (peak C in emission). Note that the first emission peak (peak A) is the direct recombination from the excited to the ground state without further relaxation (elastic peak). The energy difference between the singlet and the triplet state in NEXAFS $\Delta$ B is $\cong$ 2 eV, and singlet-CT state $\Delta$ C is $\cong$ 5 eV. Both energy differences are reproduced in the emission spectra, where the second peak appears at $\Delta$ B $\cong$ 2 eV from the elastic peak, and the third peak appears at $\Delta$ C $\cong$ 5 eV from the elastic peak. Upon dissolving the $NiCl_2$ powder in water, the CT peak in the absorption spectrum disappears (peak P3), and consequently the respective emission features disappear (peak C). To this point the absorption and the emission spectra are in a good agreement. Based on this observation, we conclude that the CT peak in solid is the finger print for the direct contact between $Ni^{2+}$ and $Cl^{-}$ interaction. Furthermore, this interaction is absent for concentrations $\leq$ 1 M $NiCl_2$.

Upon dissolving $NiCl_2$ in water, the splitting between the singlet and the triplet state in the absorption spectra increases by 0.8 eV. This increase is found in the emission spectra. At this point the changes in the spectra between the 1000 mM to the 50 mM in both absorption and emission can be explained as a decrease of the indirect contact between ions in solution. A schematic of this indirect contact is presented in Fig.4.25. We assume that at very diluted solution (50 mM) the $Ni^{2+}$ ions are surrounded by approximately six water molecules in an $O_h$ symmetry. By increasing the concentration, the $Ni^{2+}$ ions interact with the $Cl^{-}$ ions indirectly, which leads to a distortion of the $O_h$ symmetry, as was discussed in section 4.4.2, and causes an intensity rise of the singlet state relative to the triplet state. On the other hand, we can not exclude the possibility of a change in the coordination number of the water molecules around the $Ni^{2+}$ ions upon dilution. More direct structural information may thus be helpful to clarify the origin of these spectral changes.

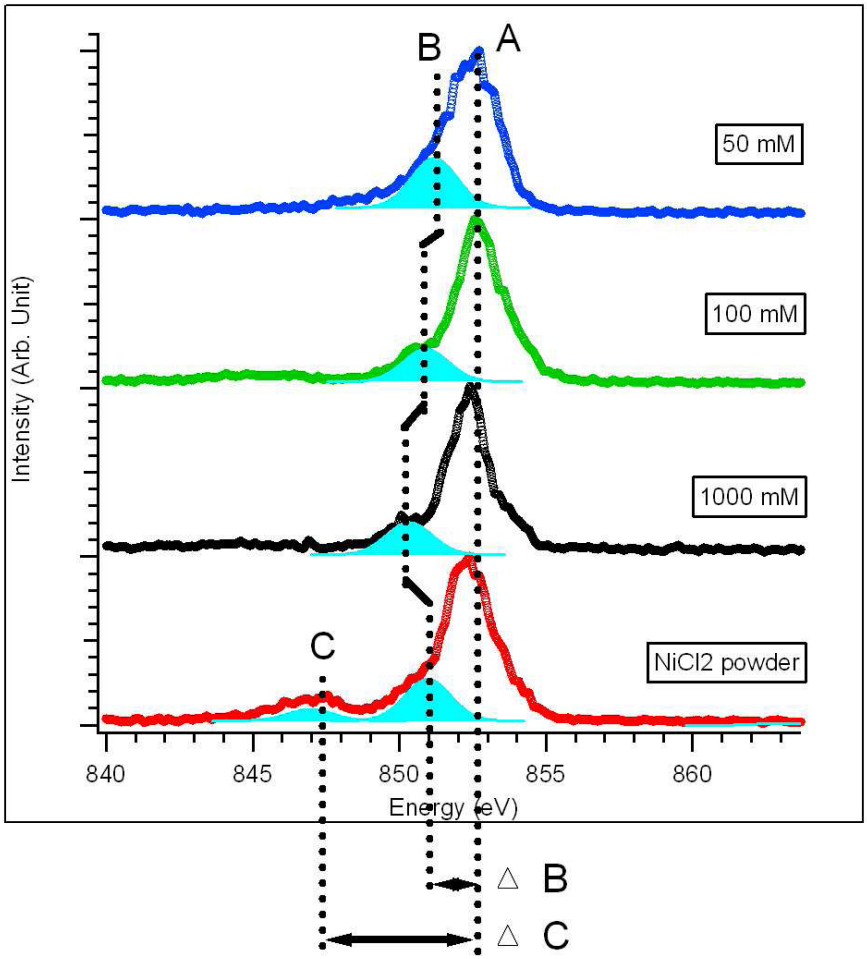


Figure 4.24: Resonant inelastic x-ray scattering for monochromatic energy correspond to the first peak of the $L_3$ absorption for $Ni^{2+}$ (852.5 eV) as a function of the concentration

### EXAFS

In order to investigate the changes in the local geometric structure around the $Ni^{2+}$ ions in water, we performed EXAFS measurements at the K-edge of $Ni^{2+}$ in the range 2000 mM down to 50 mM concentration. Reference spectrum was measured from hydrated powder, where $Ni^{2+}$ is surrounded by four water molecules and 2 $Cl^{-}$ ions. The EXAFS spectra are presented in Fig.4.26. A systematic increase in the amplitude of the EXAFS oscillation is observed upon dilution. Fourier Transformation (FT) of the EXAFS spectra with $k^3$ weighting gives the radial distribution function as shown in Fig.4.27.a. In this figure, the $Ni^{2+}$ first nearest neighbor peak (at approximately 2 $\AA$) is interpreted as

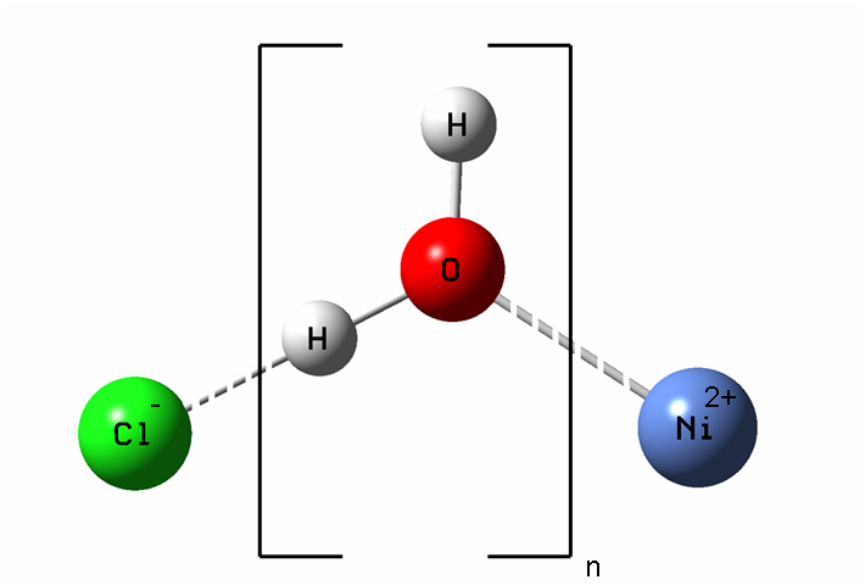


Figure 4.25: Schematic of solvent-shared ion-pair interaction between the $Ni^{2+}$ and the $Cl^{-}$. The interaction decreases upon increase of n.

the $Ni^{2+}$-water distance $d(Ni - OH_2)$. This radial distribution peak varies significantly in its intensity upon dissolving the powder in water and further dilution except for concentration range lower than 250 mM. Assuming that for the powder the area under this peak corresponds to a fourfold coordination with water, one can see that upon dissolving the powder in water, as well as diluting, the $Ni^{2+}$ coordination with water increases systematically. The radial distribution function for the hydrated powder shows a second peak at approximately 4 $\mathring{A}$. This peak can assign to the $Cl^{-}$ ion in direct contact with $Ni^{2+}$ ion. By dissolving the hydrated powder in water and form 2000 mM solution of $NiCl_2$, this peak did not affect significantly, which can be due to the ion-pairing between $Ni^{2+}$ and $Cl^{-}$ at this concentration. Upon diluting the solution, the $Cl^{-}$ peak split into two peaks. One can attribute this split to the replacement of the $Cl^{-}$ ion from the direct contact with $Ni^{2+}$ by water molecule. For the present purpose we only consider the effect of the first hydration shell in our calculation and interpretation.

We have used the FEFF8 program package to model the hydration shell. The resulting Fourier Transforms are presented in Fig.4.27.b, and the extracted

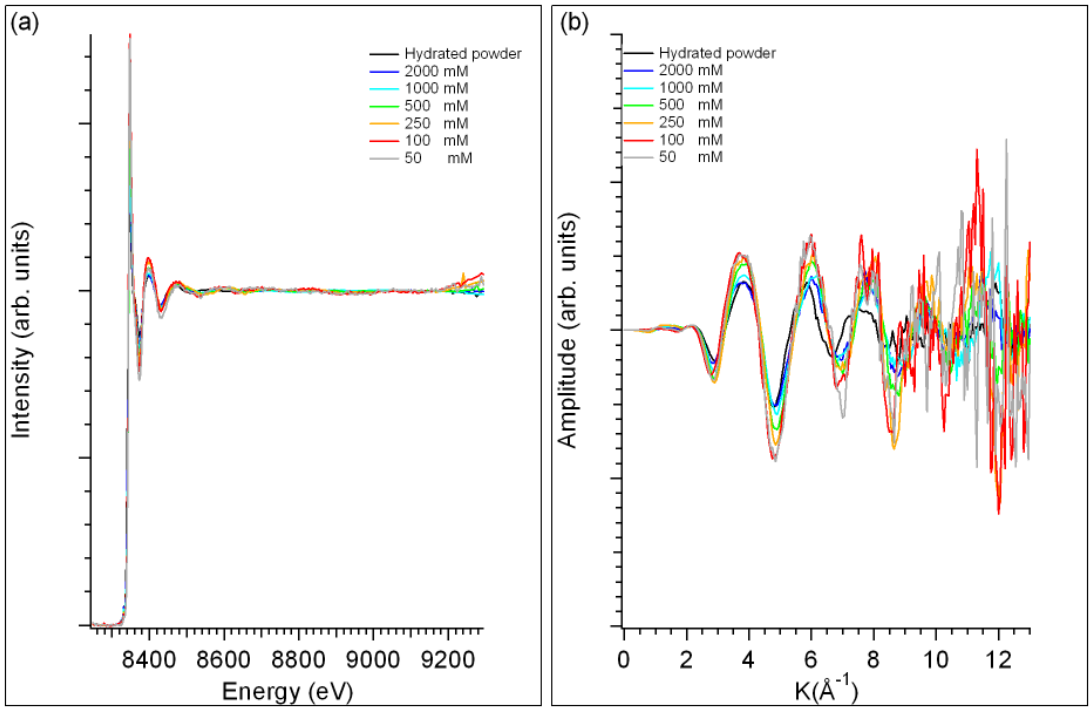


Figure 4.26: K-edge EXAFS spectra from $Ni^{2+}$ as a function of concentration, compared to the hydrated powder. The spectra are presented on energy scale (a), and on k vector scale (b)

structural data is summarized in Table.4.2. The four water coordination for the $Ni^{2+}$ powder is obtained upon fitting the experimental output with the theoretical models. In aqueous solution at 2 M, the hydration number of the water molecules increases to 4.8, and $Cl^{-}$ is likely to directly interact with the $Ni^{2+}$ at this concentration. By diluting further to 250 mM, the coordination with water increases. Further dilution from 250 mM to 50 mM shows no noticeable change in the water coordination. This is in agreement with our previous concentration dependent study on NaCl, where a decrease of the $d(Na - OH_2)$ bond length has been observed upon dilution [66].

From the EXAFS study, we conclude that there is insignificant change in the local geometry of $Ni^{2+}$ ions in water upon diluting from 250 mM to 50 mM. At concentrations higher than 50 mM, the $Cl^{-}$ ions may start to interact with the $Ni^{2+}$ ions, which causes a distortion of the $O_h$ field around the $Ni^{2+}$. At much higher concentration, $\geq$ 2 M, the direct contact between the $Ni^{2+}$ and the $Cl^{-}$ prevails. The structural information beyond the first hydration shell would be

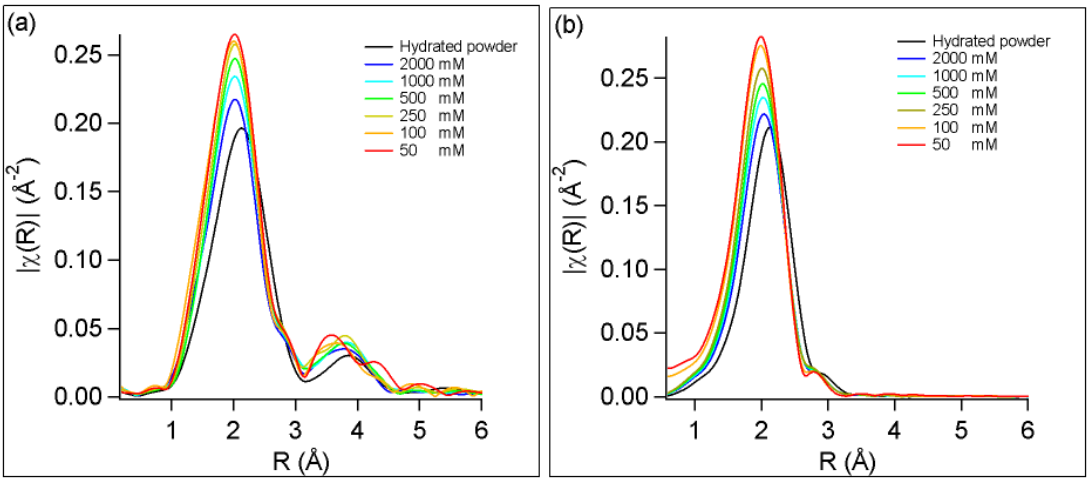


Figure 4.27: The Fourier transformed EXAFS spectra from the $Ni^{2+}$ powder dissolved in water. Data are shown for different concentration. (a) experimental data, (b) theoretical fit for the first hydration shell using FEFF8.

useful to connect the observed electronic changes to structural parameters.

| Concentration | Number of $H_2O$ | d(Ni-O) $\AA$ |
|---|---|---|
| Hydrated powder | 4.1 ± 0.1 | 2.13 |
| 2000 mM | 4.8 ± 0.3 | 2.04 |
| 1000 mM | 5.4 ± 0.2 | 2.01 |
| 500 mM | 5.8 ± 0.4 | 2.01 |
| 250 mM | 6.1 ± 0.1 | 2.01 |
| 100 mM | 6.4 ± 0.3 | 2.00 |
| 50 mM | 6.5 ± 0.2 | 1.98 |

Table 4.2: Number of water molecules in the first hydration shell, and $d(Ni - OH_2)$ obtained by fitting the experimental spectra with the calculated FEFF models of 4.2.

### 4.4.3 Conclusion

A consistent picture for the changes of the local electronic structure at $Ni^{2+}$ in $NiCl_2^{aq}$ electrolyte was developed by combining experimental L-edge $Ni^{2+}$ NEXAFS spectra with multiplet calculations of the electronic structure. While spectra for solid $NiCl_2$ exhibit an unambiguous fingerprint of charge transfer made pos-

sible by the direct Ni-Cl contact, such a feature is absent in the spectra of the electrolytes. In addition, the energy splitting between the first two absorption peaks within the $L_3$ edge (P1 and P2) is increased from 1.6 eV in the solid to 2.4 eV in the electrolyte. With increasing electrolyte concentration, the P2/P1 intensity ratio increases. These changes in peak energies and intensities are reproduced by a multiplet calculation of the Ni XANES spectra in $O_h$ symmetry by a variation of the relative contributions of the dipole matrix elements with different symmetry ($T_1$ vs. $A_2$, $T_2$ and E). This is equivalent to increase the contribution of singlet states versus the triplet states for increasing electrolyte concentration. We relate these changes in the electronic structure to the increasing importance of solvent-shared ion pairs at elevated electrolyte concentrations, manifesting itself in a progressive distortion of the local $O_h$ symmetry around the $Ni^{2+}$ ions. In order to shed more light on the changes of the local electronic and geometric structure around $Ni^{2+}$ in water, EXAFS, and RIXS were used to investigate the same system. The RIXS data confirms the changes in the electronic structural seen as a function of concentration. While the EXAFS data shows an increasing coordination of $Ni^{2+}$ ion with $H_2O$ upon dilution, no significant changes are seen between 100 mM and 50 mM in the first hydration shell. In agreement with our earlier theoretical analysis, we assign the changes at these low concentrations to the presence of indirect, solvent-shred ion pairs. Unfortunately, this could not be corroborated with the EXAFS data, as the data does not allow to extract reliable information beyond the first coordination shell in the liquid.